AD-A179 444 FORMATION AND STABILITY OF PARTIALLY-NEUTRALIZED PLASMA 1/1
CLUMPS(U) MARYLAND UNIV COLLEGE PARK LAB FOR PLASMA AND
FUSION ENERGY STUDIES J GUILLORY 01 JAN 87
UNCLASSIFIED AFOSR-TR-87-0477 AFOSR-86-0055 F/G 20/9 NL

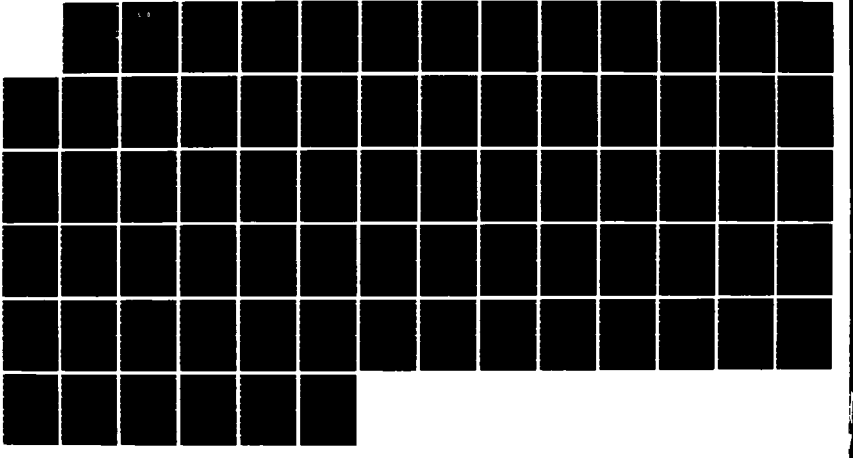

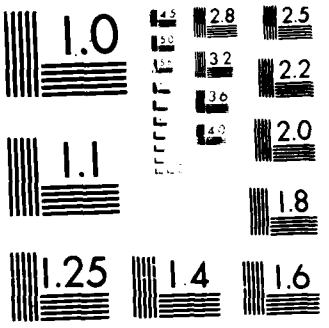

UNCLASSIFIED

AD-A179 444

DTIC FILE COPY

REPORT DOCUMENTATION PAGE

DTIC ELECTE APR 02 1987 S D

1a. SECURITY CLASSIFICATION: Unclassified	1b. RESTRICTIVE MARKINGS
2a. SECURITY CLASSIFICATION AUTHORITY	3. DISTRIBUTION/AVAILABILITY OF REPORT: Approved for public release; distribution unlimited
2b. DECLASSIFICATION/DOWNGRADING SCHEDULE	
4. PERFORMING ORGANIZATION REPORT NUMBER(S)	5. MONITORING ORGANIZATION REPORT NUMBER(S): AFOSR-TR- 87-0477
6a. NAME OF PERFORMING ORGANIZATION: The University of Maryland	6b. OFFICE SYMBOL (If applicable):
6c. ADDRESS (City, State and ZIP Code): Univ. of Maryland, College Park Campus, Laboratory for Plasma and Fusion Energy Studies/ Energy Research Bldg, College Park Md 20742	7a. NAME OF MONITORING ORGANIZATION: AFOSR 7b. ADDRESS (City, State and ZIP Code): Bldg 410, Bolling AFB, D.C. 20332-6448
8a. NAME OF FUNDING/SPONSORING ORGANIZATION: AFOSR	8b. OFFICE SYMBOL (If applicable): NP
8c. ADDRESS (City, State and ZIP Code): same as 7b.	9. PROCUREMENT INSTRUMENT IDENTIFICATION NUMBER: AFOSR-86-0055

10. SOURCE OF FUNDING NOS.

PROGRAM ELEMENT NO.	PROJECT NO.	TASK NO.	WORK UNIT NO.
61102F	2301	A7	

11. TITLE (Include Security Classification): "FORMATION AND STABILITY OF PARTIALLY-NEUTRALIZED PLASMA CLUMPS"

12. PERSONAL AUTHOR(S): Dr. John Guillory

13a. TYPE OF REPORT	13b. TIME COVERED	14. DATE OF REPORT (Yr., Mo., Day)	15. PAGE COUNT
Annual	FROM 86/01/01 TO 86/12/01	87 January 1	72

16. SUPPLEMENTARY NOTATION

17. COSATI CODES			18. SUBJECT TERMS (Continue on reverse if necessary and identify by block number)
FIELD	GROUP	SUB GR	collective Accleration, Plasmoids, Electron Beams

19. ABSTRACT (Continue on reverse if necessary and identify by block number)

Experimentally a University of Maryland group has investigated neutralized electron beam propagation in nonconducting vacuum drift tubes (to eliminate image currents and a clear return path for the electrons) and investigated a significant new way of increasing the ion velocity (and therefore the propagation distance) in such systems. In thisprogram the investigators have constructed a microscopic equilibrium for such a propagating electron/ion beam in which both species are in radial force balance, and they have begun numerical simulation studies of bean and ion propagation in such a system.

20. DISTRIBUTION/AVAILABILITY OF ABSTRACT	21. ABSTRACT SECURITY CLASSIFICATION
UNCLASSIFIED/UNLIMITED ☐ SAME AS RPT ☒ DTIC USERS ☐	UNCLASSIFIED

22a. NAME OF RESPONSIBLE INDIVIDUAL	22b. TELEPHONE NUMBER (Include Area Code)	22c. OFFICE SYMBOL
BRUCE L. SMITH	(202)767-4907	NP

DD FORM 1473, 83 APR EDITION OF 1 JAN 73 IS OBSOLETE. UNCLASSIFIED

SECURITY CLASSIFICATION OF THIS PAGE

ANNUAL TECHNICAL REPORT

FORMATION AND STABILITY OF PARTIALLY-NEUTRALIZED PLASMA CLUMPS

Grant No. AFOSR-86-0055
For the period
January 1, 1986 to December 15, 1986

Submitted to
Air Force Office of Scientific Research
January 1987

Prepared by
Laboratory for Plasma and Fusion Energy Studies
University of Maryland
College Park, MD 20742

RESEARCH PROGRESS AND FORECAST REPORT

Submitted to:	Air Force Office of Scientific Research
Submitted by:	Laboratory for Plasma and Fusion Energy Studies University of Maryland College Park, MD 20742
Grant Number:	AFOSR-86-0055
Period:	January 1, 1986 to December 15, 1986
Principal Investigators:	John Guillory, Senior Research Associate Martin P. Reiser, Professor Charles D. Striffler, Professor
Title of Research Project:	Formation and Stability of Partially-Neutralized Plasma Clumps

PROJECT SUMMARY

PROJECT TITLE: Formation and Stability of Partially-Neutralized Plasma Clumps

CONTRACT/GRANT NO: AFOSR-86-0055 CONTRACT/GRANT VALUE: $44,662
CONTRACT/GRANT PERIOD OF PERFORMANCE: 1 January-15 December 1986

PRINCIPAL INVESTIGATOR(s): J. Guillory TEL #: 454-7102; 671-2333
M. Reiser, C. Striffler TEL #: 454-3188; 3183

BUSINESS MAILING ADDRESS: Laboratory for Plasma and Fusion Energy Studies
University of Maryland
College Park, MD 20742

RESEARCH OBJECTIVE:

Theoretical and numerical studies of plasmoid shedding from gas puffs and virtual cathodes; and stability of plasma clumps traversing low-density plasma background.

APPROACH:

Analytic and numerical analysis of time-dependent electron and ion emission from downstream side of a plasma puff subjected to an electron beam pulse; analytic and numerical analysis of equilibrium and stability of a bounded, relatively dense plasma in a tenuous background by treating the background as "beam" in the plasma frame.

This report describes the first year of the suggested two-year effort.

TABLE OF CONTENTS

1. INTRODUCTION

Studies of the propagation of intense charged particle beams into vacuum have been pursued at the University of Maryland under AFOSR sponsorship since 1984. That program has been investigating under what conditions intense charged particle beam energy may be propagated into free space without the benefit of confining magnetic fields or conducting boundaries. Experimental and theoretical work has centered around the propagation of intense electron beams into vacuum after passage through an ion source localized near the injection point. In such systems propagation can occur when ions are accelerated from the source region into vacuum by the space charge fields of the electron beam. The resultant neutralization of the electron beam by the accelerated ions allows effective propagation in the vacuum region, to the extent studied in the experiments. The goal of that related work is the generation of nearly charge-neutral, current-neutral charged particle beams which are capable of propagating beam energy in vacuum at a significant fraction of the velocity of light.

From the related work in our group, we have arrived at the following understanding of the dynamics when an intense electron beam is injected into vacuum through a localized plasma source:

(a) At the beginning of electron beam injection, a virtual cathode is established in the region of the localized plasma source. The electric field associated with the virtual cathode reflects the electrons and accelerates the ions to a mean kinetic energy equal to the electron beam energy, eV_0.

(b) After acceleration, the bulk of the ions drift with a mean velocity $v_i = (2eV_0/m_i)^{1/2}$.

(c) As a quasi-steady ion flow is established, the virtual cathode moves a short distance downstream and then remains at this new position.

(d) During the motion of the virtual cathode to its new position, a group of ions in phase with the moving potential well gains additional kinetic energy $q\bar{E}\Delta z$ where $\bar{E}$ is the average electric field associated with the virtual cathode and Δz is the displacement distance of the virtual cathode. This phenomenon represents an explanation for the so-called "high-energy tail" in the ion distribution observed in the experiment.

(e) A large fraction of the injected electrons are reflected at the displaced virtual cathode. The rest propagate together with the ions that form a charge-neutralizing channel. The equilibrium state of the self-focused electron-ion beam propagating downstream has been studied. The initial results of that study are presented in a paper to be published in the proceedings of the Beams 86 Conference (see Appendix A). Improved results were presented at the 1986 Plasma Physics Meeting (see Appendix A).

(f) It appears that a second virtual cathode forms at the beam front from which most of the propagating electrons are reflected.

The purpose of this related study, begun in January 1986, is to model and analyze the formation of partially neutralized plasma clumps emitted from such an ion-source plasma traversed by an electron beam, and

to analyze the stability of such plasmoids propagating in a very low-density plasma background. It is convenient, for this first annual report, to divide our analysis into the following sections:

2. Formation - 1D equations and simulation.
3. Formation - 2D effects.
4. Characterization of source plasma.
5. Stability of propagating plasmoid-linear theory.
6. Stability of propagating plasmoid-nonlinear theory.

These tasks reflect a level-of-effort of 1/6 MY of Dr. Guillory from 1/2/86 to 10/31/86, and about 1/6 MY of Dr. Yao and Dr. Guillory from 11/1/86 to 12/15/86 once Dr. Yao, a postdoctoral fellow, was acquired for the grant research. (The second-year level of effort is expected to be enhanced to allow timely completion of the proposed research objectives.)

In this first annual progress report for this program, we report significant new theoretical results. Experimentally the University of Maryland group has investigated beam propagation in such systems in nonconducting vacuum drift tubes (to eliminate image currents and a clear return path for the electrons) and investigated a significant new way of increasing the ion velocity (and therefore the propagation distance) in such systems. In this program we have constructed a microscopic equilibrium for such a propagating electron/ion beam in which both species are in radial force balance, and we have begun numerical simulation studies of beam and ion propagation in such a system.

Our primary goals for the remaining one-year period are to analyze further the formation and instability limitations of such plasmoids, which are seen as a means of propagating appreciable particle energy densities in vacuum. Sections 2-6 of this report outline progress made in our studies during the 1986 grant period.

2. FORMATION - 1D

2.1 Ion Motion

Previous 1-D particle codes [Dantsker et al., Bull. APS 29, 1353 (1984)] have indicated that most of the ions (and electrons) follow each other along a single phase-space trajectory. This implies that a fluid model may be adequate for a 1-D description of the accelerated motion of the plasma ions as they leave the ionizing source plasma. To this end, we then begin with the following simple 1-D fluid model for the ions:

$$(\partial_t + v_i\partial_z)v_i = \frac{e}{m_i} E \ ,$$

$$\partial_t n_i + \partial_z(n_i v_i) = S_i(z) \ ,$$

$$\partial_z E = 4\pi e(n_i - n_b) \ ,$$

with $n_i(t = 0) = n_{i0}e^{-z/\ell}$, ℓ = gas puff scale-length. Here $S_i(z)$ is the ionization source rate, and n_b must be coupled to E.

To simplify the expansion of this ion plasma even further, let us assume ℓ is small, neglect the production of new ions (i.e., take S_i = 0), and look for a self-similar expansion. Letting $x = z/v_0t$ be the similarity variable, where v_0 is the ion velocity when given the input beam-electron energy E_0. Rewriting the above equations in the dimensionless variables,

$$u = v_i/v_0 \ ,$$

$$\psi = e\phi/E_0 \ ,$$

$$n = n_i/(n_b \text{ at } \psi = 0) \ ,$$

and using the similarity condition, one arrives at

$$(u - x)\frac{dn}{dx} + n\frac{du}{dx} = 0 \ ,$$

$$\frac{d\psi}{dx} + (u - x)\frac{du}{dx} = 0 \ ,$$

and we require some form $n(\psi)$ for the ions and beam (the resulting plasma expansion is quasineutral). For simplicity of results we assume

$$n(\psi) = (1 + \psi)^p$$

with p an adjustable power (typically, experiments indicate $p \sim 3$). The solution of this simplified set of ODE's is

$$u = u_0 + ax \ ,$$

$$n = p^p[u_0 - (1 - a)x]^{2p}$$

$$\psi = p[u_0 - (1 - a)x]^2 - 1 \ ,$$

with $a = 1 - (2p + 1)^{-1/2}$ and $u_0 = 2^{1/2}(2p + 1)^{-1/2}$, from ion energy conservation, $u^2/2 + \psi \approx$ const. $= 0$ at $x = 0$ out to $x = u_0/(1 - a) = \sqrt{2}$, where n goes to zero.

The peak ion kinetic energy, $1/2\ u^2$ at $x = u_0/(1 - a)$, is unity, i.e., ions at the head of the expansion have the full electron beam-input energy. When electron energy loss to the potential is included, the value of a increases and the peak ion kinetic energy can be somewhat larger.

The transient introduction of the electron beam leads to an oscillatory transient, damping to such a self-similar expansion. Such transients, the subject of part of our second-year effort, are intimately related to the electron dynamics, and are important if large, because they may determine the size of emitted plasmoids.

2.2 Electron Motion

To model the beam and sheath electron disturbances at the exit-surface of a relatively cold dense plasma traversed by the electron beam, we begin with the 1-D model system

$$\partial_z^2(e\phi) = 4\pi e^2(n_e + n_b - n_i) ,$$

$$\partial_t n_e + \partial_z(n_e v_e) = S_e ,$$

$$\partial_t v_e + v_e \partial_z v_e = \partial_z\left(\frac{e\phi}{m}\right) .$$

Here we let $\tau = \omega_{pb}(0)t$, $x = z/h_n$ where h_n is the "initial" or typical density gradient scale height, and $u = v_e/h_n\omega_{pb0}$. In terms of these dimensionless variables and

$$\psi = \frac{e\phi}{mh^2\omega^2 n_{pb0}} ,$$

$$N_e = n_e/n_{b0} , \quad N_i = n_i/n_{b0} ,$$

the above equations become

$$\partial_x^2 \psi = N_e - N_i + I(\psi) ,$$

$$\partial_\tau u = \partial_x \psi ,$$

$$\partial_\tau N_e + u\partial_x N_e + N_e \partial_x u = \tilde{S} ,$$

where we have neglected $v_e \cdot \nabla v_e$ compared with $\partial_t v_e$.

This set of equations purports to describe space charge oscillations in the non-quasineutral sheath of the quasi-stationary-ion plasma, i.e., it is intended as a fast-timescale fluid description of the electron sloshing. The function $I(\psi)$ simply describes the profile in x of the beam electron density, and is normalized to unity at x = 0. For a uniform beam (reflexing or not), I = 1. N_i is specified, in a way consistent with the ion slow-timescale equations, e.g., the self-similar model treated above, or some more general one.

Analysis (and/or generalization) of this 1-D electron-motion/space-charge oscillation model is part of our projected second-year effort, as is computer simulation. When the electron beam is modulated in time (even if only by its rise and decay) we expect that the large-amplitude space-charge oscillations near the forward edge of the quasineutral expanding plasma can lead to modulation of the ion flow. We cannot yet

predict the relative phases of the ion and electron modulation (jetting?), although energetics would tend to favor in-phase (quasineutral) clump formation.

In Fig. 1 a schematic of the model described in Secs. 2.1 and 2.2 is shown. The electron beam is shown incident onto the plasma source region and the resulting virtual cathode forming just beyond the downstream plasma surface. An early time profile of the potential is displayed and the indicated movement of the potential profile to the downstream plasma surface. The sheath region, from which ions are emitted, is also displayed on the downstream plasma surface. Ions are drawn out of this region and form schematically the indicated spatial profile.

2.3 1-D Simulations

The numerical model of our localized plasma source-beam propagation system is shown in Fig. 2a. A solid electron beam of radius R_b, current $I_0 = J_0 \pi R_b^2$, and voltage $eV_0 = mc^2(\gamma_0 - 1)$ is injected through one end of an evacuated drift tube of radius R_w and length L. The entire system is immersed in a magnetic field that is sufficiently large to impede any radial expansion. Without the presence of a source of ions, a deep potential well of depth about equal to the voltage V_0 forms in a region about 1-2 mm from the entrance end when the injected current is above the space-charge limiting current

$$I_L = \frac{17(\gamma_0^{2/3} - 1)^{3/2}}{1 + 2\ell n(R_w/R_b)} \text{ kA} .$$

In this case the majority of the incoming beam particles are reflected

FORMATION - 1D

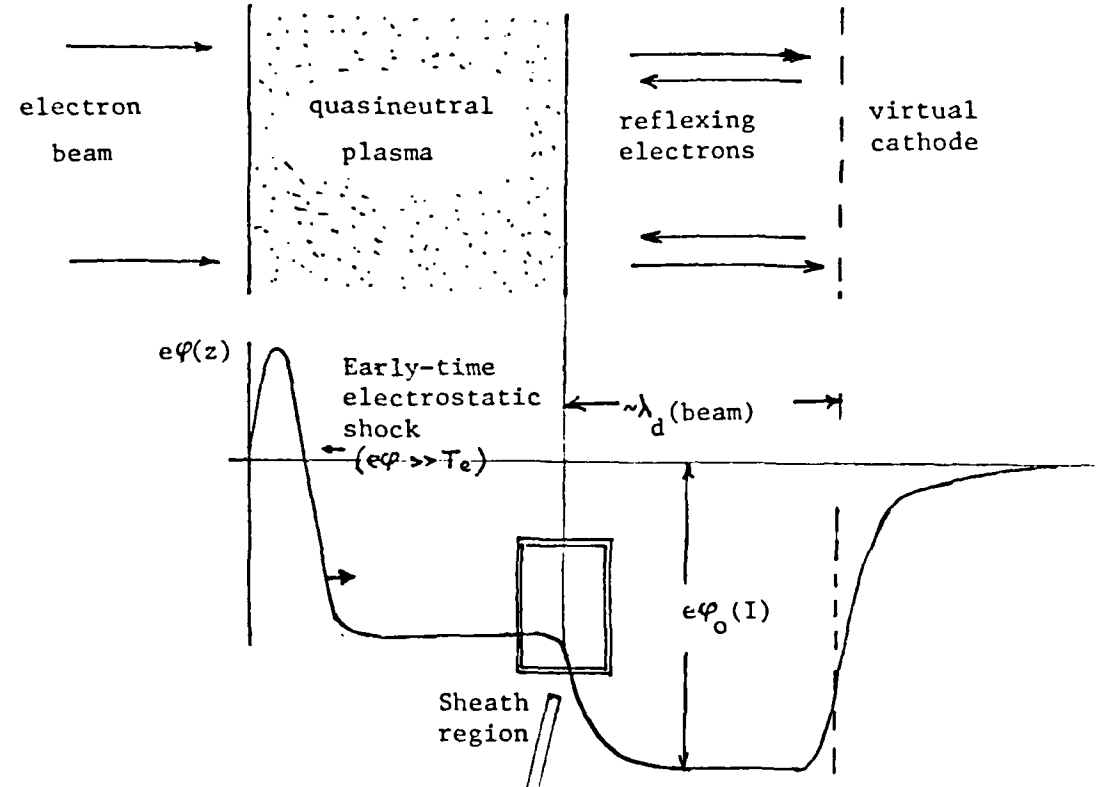

Sheath region:

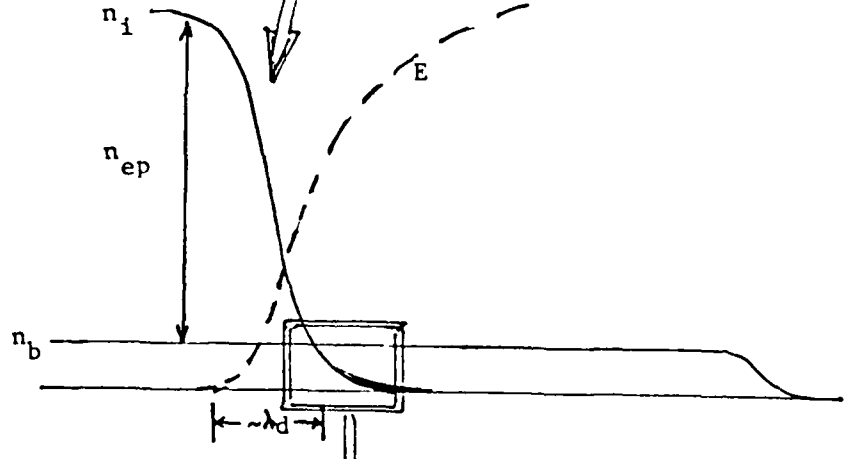

Ion model:

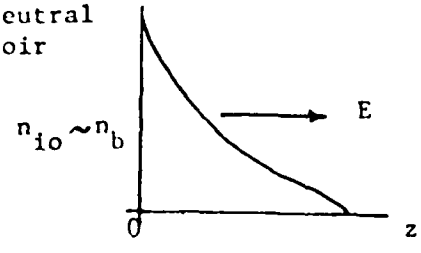

$$(\partial_t + v_i\partial_z)v_i = \frac{e}{m_i}E \quad ; \quad \partial_z E = 4\pi e(n_i - n_b)$$

$$\partial_t n_i + \partial_z(n_i v_i) = 0$$

$$n_i = n_{io}e^{-z/L} \quad , \quad L \sim \lambda_d$$

FIG. 1. Schematic of localized plasma-electron beam system

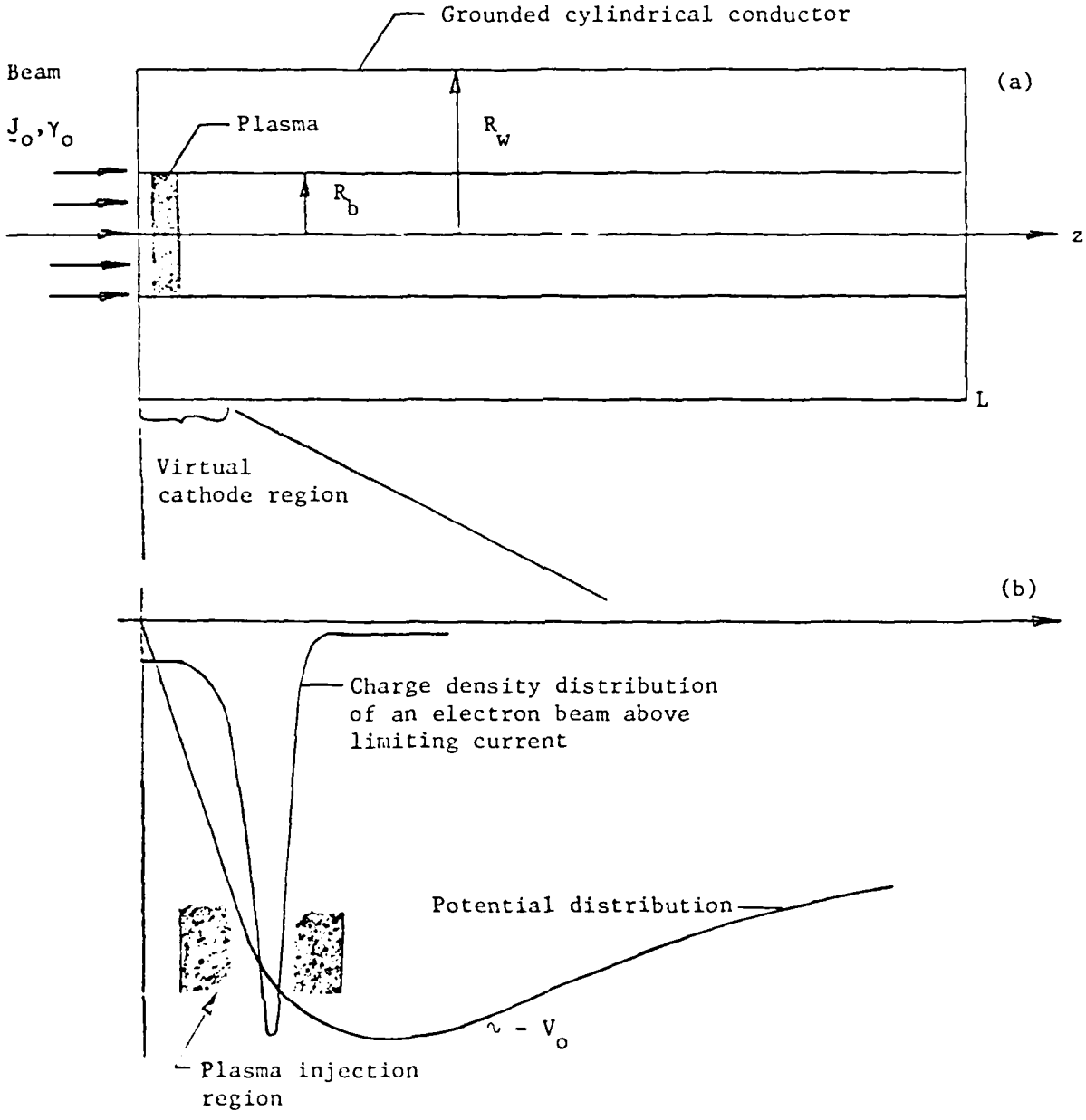

FIG. 2. Geometry and schematic of CIA model.

back to the anode (z=0) by this deep potential well and a fraction are transmitted past it.

In Fig. 2b, we have pictorially shown where plasma is formed due to the presence of a cloud of gas localized to the region near the entrance end. This cloud of gas is ionized by the electron beam and subsequently by the plasma particles (ions and electrons) and serves as the source of ions that enables the beam to propagate further downstream. The development of the code (J. Grossmann's Ph.D. thesis, 1982) and a prescribed rate of plasma formation had been the model studied during the initial phases of research. In 1984, we quantified the ionization process. This model is described below and results shown of the initial runs with our electrostatic code [(r,z) geometry; p_z momentum].

A neutral gas is assumed to occupy a region close to the anode. Specifically

$$p(z) = \begin{cases} p_0 , & 0 \leq z \leq z_0 \\ 0 , & z_0 < z \leq L \end{cases} ,$$

where p(z) is the pressure of the gas in torr. The formation of plasma particles via ionization is given in terms of a cross-section of the interaction. Mathematically the formation of plasma particles (ions and electrons) in a time Δt is given by

$$\Delta N_{pi} = \Delta N_{pe} = \sum_{\alpha} S_{\alpha}(KE_{\alpha}) \times v_{\alpha} \times \Delta t \times p \times N_{\alpha} \text{ particles}$$

where S_{α} is the number of ionization events per cm per torr, v_{α} and KE_{α}

are velocity and kinetic energy of the ionizing particle resulting in the ionization, and N_α is the number of particles of type α. The sum over species α represents the contribution to ionization by beam electrons, accelerated plasma ions, and plasma electrons. The time Δt is chosen as the time step of the simulation and ΔN is calculated for each mesh region Δz separately. When a sufficient number of plasma particles have been formed in a mesh region a macroparticle of that type is released into the system and is subsequently accelerated by the electric field. This particle is then also allowed to ionize the gas. The specific expressions for S_α incorporated into the numerical model are:

$$S_e = \begin{cases} 0 & KE_e < 20 \\ \sqrt{10} & 20 \leq KE_e \leq \sqrt{10} \times 10^2 \\ e^{6.91/KE_e} & \sqrt{10} \times 10^2 \leq KE_e \leq 10^5 \\ 10^{-2} & 10^5 \leq KE_e \end{cases}$$

and

$$S_i = \begin{cases} 0 & KE_i < 10 \\ e^{2.383 \log_{10} KE_i - 8.577} & 10 \leq KE_i \leq 4.3 \times 10^4 \\ e^{-1.839 \log_{10} KE_i + 11.036} & 4.3 \times 10^4 \leq KE_i \end{cases}$$

where KE_α is expressed in terms of eV and these expressions model the curves given in the reference C. L. Olson, V. Schumacher, Collective Ion Acceleration, Springer Tracts #84, 1979, p. 50.

The results of our numerical simulation incorporating the ionization process described above are shown in the set of plots in Figs. 3(a)-3(c). The system and beam parameters are listed in the figure caption for Fig. 3(a). Note the following points:

- The t = 0.3 ns plots show the potential depression region due to the high current electron beam. That is, near z ~ 1-2 mm the beam electrons are reflected back to the anode and only a few are transmitted downstream. This latter number represents the limiting current $I_L \sim 2$ kA. These plots also show how and where plasma particles are formed. That is, they are forming near the potential minimum since the rate of ionization is largest when the beam electrons have a relatively low velocity.

- The $t \geq 3$ ns plots show the results for the entire tube length. The potential depression $\phi \sim -V_0$ is restricted to the anode region early in time but broadens as time increases. At the same time ions move downstream, the region of broadening being about equal to the extent of the region occupied by the ions.

- The ions at the front of the broadened region have an energy of about 2 MeV, i.e., four times the beam energy in the diode. The bulk of the ions have an energy between 0.5 and 1.0 MeV. This increase above 0.5 MeV appears to be due to the positive potential region restricted to the gas cloud region. This positive potential oscillates about 0.2 MV.

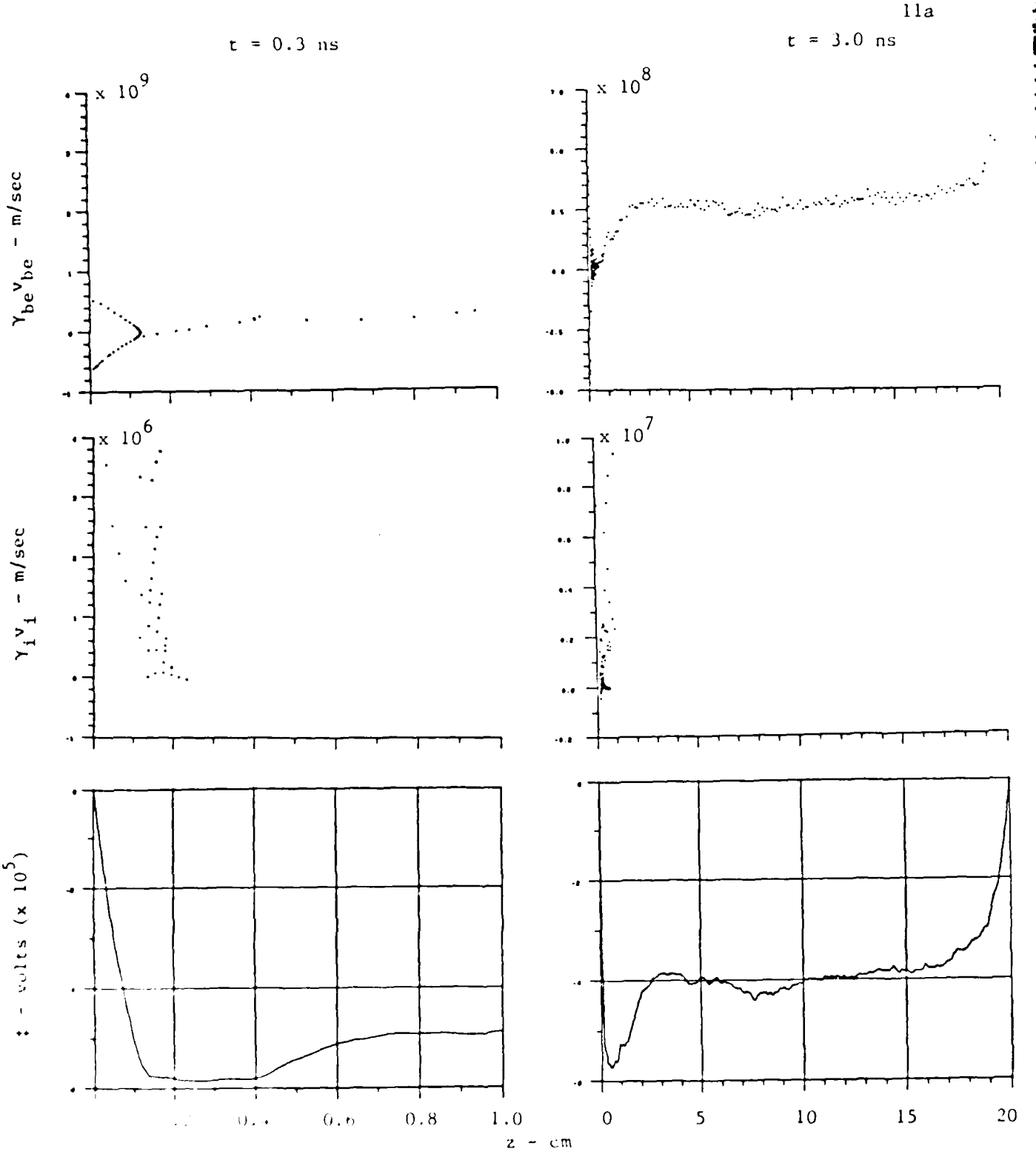

... Phase-space plots of beam electrons and plasma ions, and potential ... at time t = 0.3 ns and 3.0 ns. The system parameters are: L = 20 cm, ... The beam parameters are: $\gamma_0 = 2$ ($V_0 = 0.511$ MV), $R_b = 0.5$ cm, ... = I_p. The neutral gas parameters are: $p_0 = 0.5$ torr, $z_0 = 1$ cm. ... parameters are: $\Delta z = 0.1953$ mm, $\Delta t = 0.7523$ ps. Macroparticle ... are: $N_{pb} = 1 \times 10^{11}$, $N_{pi} = N_{pe} = 0.5 \times 10^{11}$, $\Delta z_i = \Delta z$.

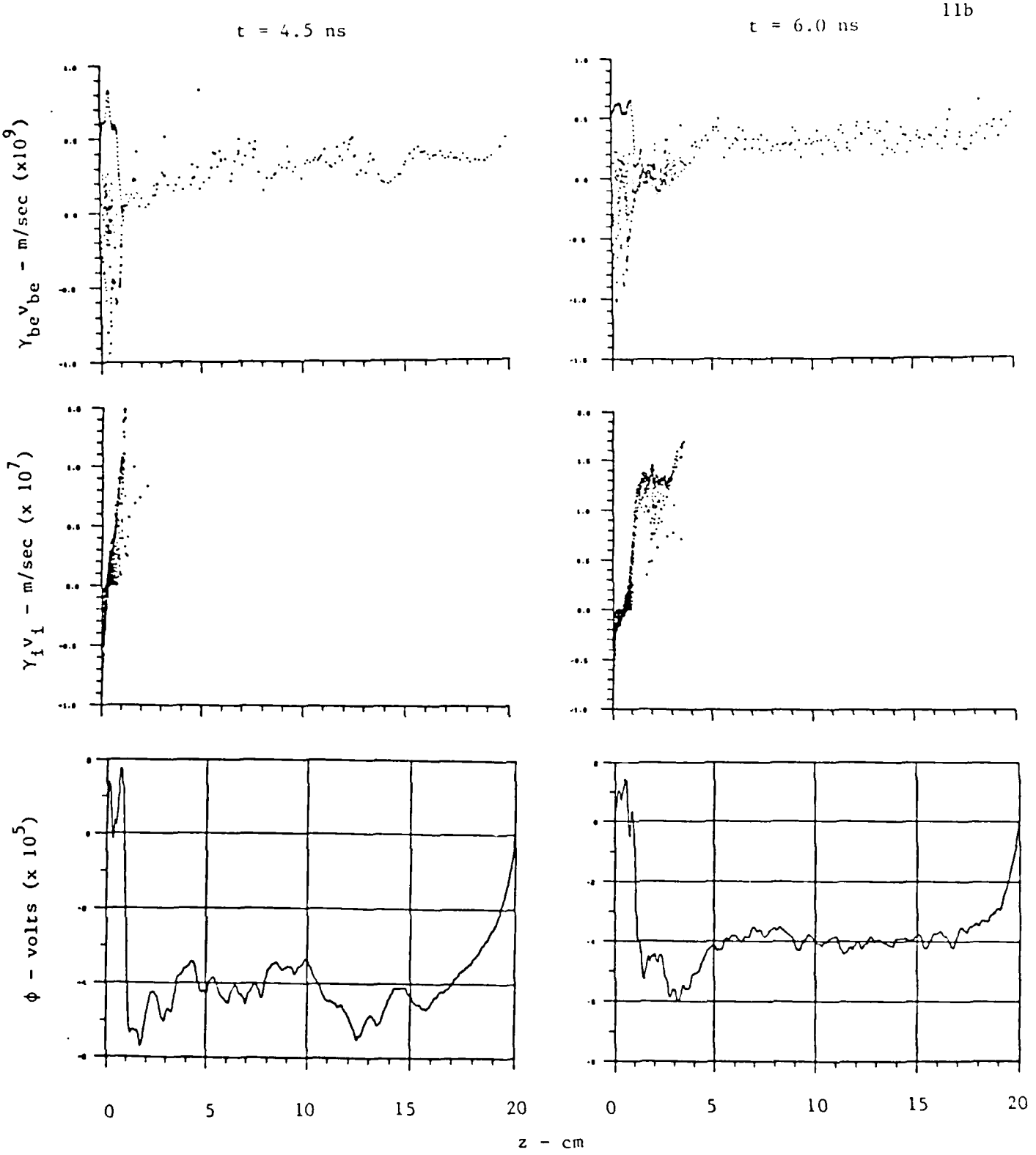

FIG. 3(b). Same as Fig. 3(a) except t = 4.5 ns and 6.0 ns.

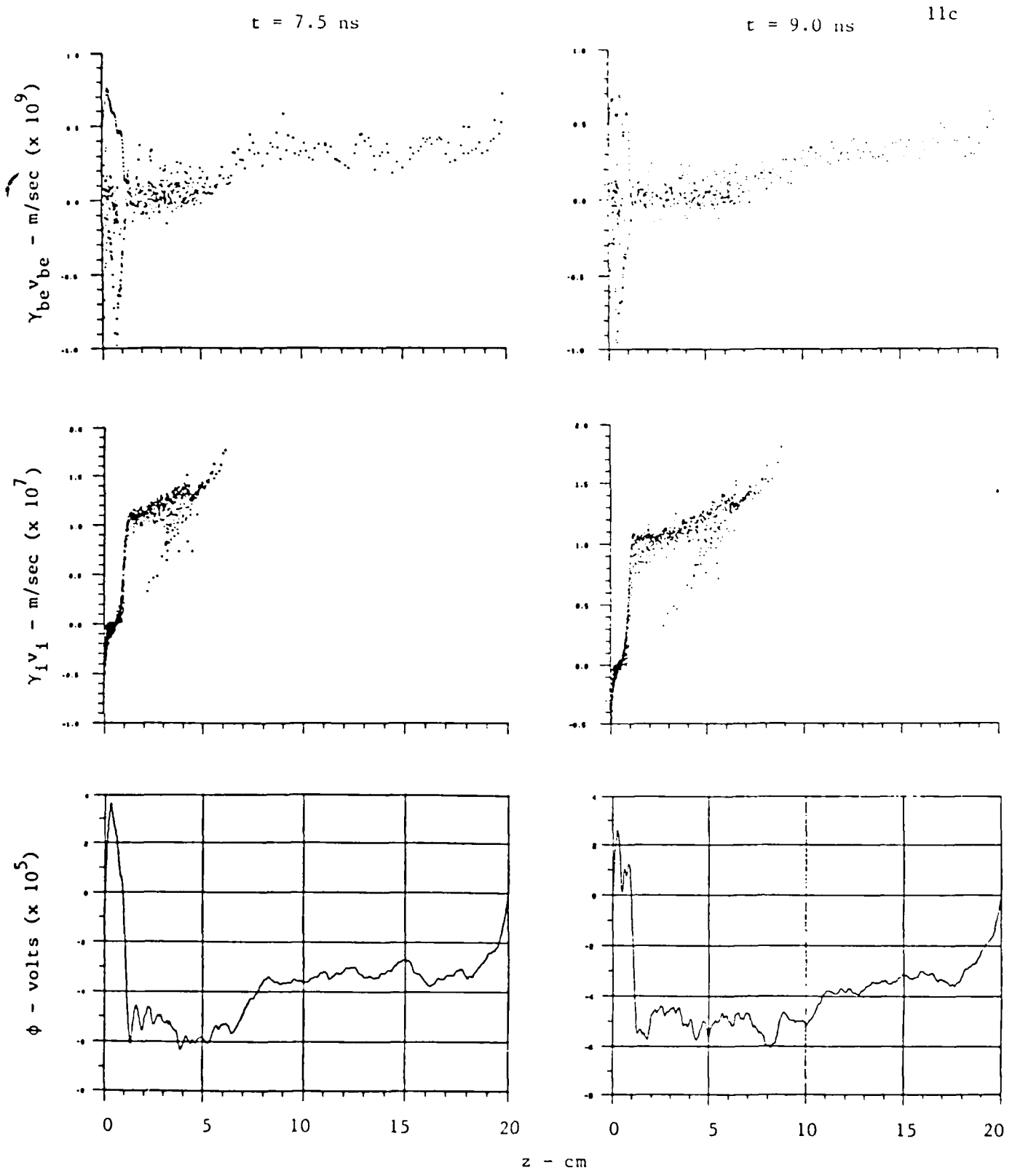

FIG. 3 (c). Same as Fig. 3 (a) except t = 7.5 ns and 9.0 ns.

- For $t \gtrsim 4.5$ ns the steep gradient in potential remains near the end of the gas cloud region for this gas pressure. However, though there is no further increase in the peak ion energies, the ions are still supplied to the beam front for beam propagation purposes.

- By keeping count of the number of plasma particles formed, we find that no movement of the deep potential region occurs until ionization by the plasma ions becomes important, i.e., until avalanching occurs.

The results shown here represent a great improvement on our previous numerical studies, mainly because of the quantification of the gas cloud region. Further studies will be performed during the second year of this research.

3. FORMATION - 2D EFFECTS

3.1 Analytic Theory

A current-carrying, ablating planar plasma is subject to a thermal-resistive instability when inelastic-collision smoothing of temperature gradients is not dominant (Tripathi, Ottinger, and Guillory, 1983). Hotter regions carry more current and heat further, under a range of circumstances. This leads to radial (or otherwise transverse) inhomogeneities of the exit surface of the source plasma, on a timescale that can be approximately the same as the beam risetime (~ 10 ns in the Maryland experiments). In the first year of this grant research, we have coupled the first-order (linearized) perturbations in density and temperature to the axial ion motion, i.e., we have analyzed the ion motion response as driven by the unstable electron currents. And we have generalized the perturbation equations of the instability analysis to allow for axial gradients in the equilibrium density, temperature, etc.

In order to explore the filamentation and jetting of a plasma "slab" through which an electron beam is passing, we have derived linear perturbation equations for the low-frequency oscillations in a quasineutral plasma with gradients in the axial direction. The rationale for this is that transverse filamentation and axial jet structures may determine the size of quasineutral plasma clumps shed from the downstream edge of the plasma. There is both theoretical and experimental evidence that such transverse disturbances may occur in the cathode blowoff plasma of energetic electron beam diodes (Tripathi, Ottinger, and Guillory, 1983; Stephanakis, Goldstein, and Mosher, 1982).

The perturbation equations comprise a set of coupled ordinary differential equations in z, with complex eigenfrequency ω, for the perturbation eigenfunctions of density, current, temperature, and fields. As a first step we have analyzed the ion response as driven by the unstable electron current perturbations.

The model is as follows: a quasineutral plasma initially uniform in x and y has a density falloff in z with scale length κ_n^{-1}. The z-directed fluid velocity v in the plasma has a scale length κ_v^{-1} in z. The z-directed ion fluid velocity v_i has the same scale length, κ_v^{-1}. There may also be electron temperature gradients in z, with scale length κ_T^{-1}. The ions are cold. Through this plasma streams an energetic electron beam, which travels with only (+ and -) z-directed motion and extends uniformly in z beyond the plasma. There is a magnetic field in the y-direction due to the electron current. We perturb the equations of this plasma with a perturbation varying as $\exp(ik_x x + ik_y y - i\omega t)$, but with phase velocity $\ll c$. We assume the perturbed ion and electron densities are equal (quasineutral perturbations). The beam electrons are assumed unperturbed in their brief transit through the perturbations in the plasma. Collisions, including inelastic collisions are included in the finite-resistivity plasma model, although they become negligible where the density becomes small. This is because we know from our previous work with a uniform plasma slab model that inelastic electron collisions affect the stability of the system (Tripathi, Ottinger, and Guillory, 1983). The plasma is assumed to have a small charge imbalance compensating the electron beam space charge, and this charge imbalance is not negligible where the density is low. It couples with the electric field $\vec{E}$ to give a self-consistent force in addition to the $J \times B$ and ∇P

forces.

The perturbed quantities are thus n, $\rho = n_i - n_e$, $T(= T_e)$, v, $J(= J_y)$, $\vec{E}$ and $\vec{B}$. But since perturbations of the form $\rho_i E_0$ and $\rho_0 E_1$ give rise to high frequency electron plasma waves to which the ions cannot respond except as a nonlinear ponderomotive matter, we ignore them in this particular analysis. (We consider ponderomotive ion acceleration elsewhere.)

In its simplest form, the thermal-resistive instability displays the growth rate

$$\gamma \sim \frac{kc}{\omega_{pe}} \nu_0 \left[\frac{\nu_0 \varepsilon_{drift} \cdot 4\cos^2\vartheta}{\left(\frac{3}{2} + \frac{\partial}{\partial(\ell n T)}\right)\dot{\varepsilon}_{coli}} - 1\right]$$

with the definitions:

$$\nu_0 = \text{electron collision rate}$$

$$\varepsilon_{drift} = \frac{1}{2} m v_e^{-2}$$

$$\cos\vartheta = "\kappa_z"/\kappa \qquad\qquad \kappa_z \sim \frac{1}{n}\frac{\partial n}{\partial z}$$

$$\dot{\varepsilon}_{coll} = \text{inelastic-collision energy loss rate of electrons (proportional to radiation per electron)}$$

Coupling the perturbations of E field and electron temperature to perturbed <u>ion</u> motion, we get, e.g., for the perturbation amplitude of axial ion velocities

$$\frac{v_{iz_1}}{c_s} \approx \frac{\gamma\ell}{c_s}\left\{\frac{\left(\frac{n_b}{n_0}\right)\left(\frac{\ell e E_1}{T_e}\right) - [(1 + iK_z)(1 + s) + rs]\left(\frac{T_1}{T_e}\right)}{K^2 - (\gamma\ell/c_s)^2 - iK_z(2 + r) - (1 + r)}\right\}$$

with the definitions

$$\ell = \left(\frac{1}{n}\frac{\partial n}{\partial z}\right)^{-1}, \quad \kappa_{(z)} = k_{(z)}\ell, \quad r = \frac{\ell}{T_e}\frac{\partial T_e}{\partial z}, \quad s = \frac{\partial(\ell n n)}{\partial(\ell n T_e)}_{\text{ionization}},$$

and with E_1 and T_1 the electric field and electron temperature perturbations.

3.2 2-D Code

We have loaded onto the local computer the 2-D, fully-electromagnetic particle code WAVE, originated at Los Alamos for the study of hot electron (etc.) dynamics near the absorption of laser light in an ablating plasma.

The WAVE code solves Maxwell's equations and particle equations of motion on a Cartesian mesh with a variety of field and particle boundary conditions. Although it has been used primarily to study the interaction of intense laser light with plasmas, it has the capability of studying many other phenomena including shock waves, beam plasma instabilities, etc. It was first written by R. L. Morse and C. W. Nielson in 1971, improved by C. W. Nielson and E. L. Lindman, maintained by D. W. Forslund (with the addition of highly optimized disk I/O routines), and recently modified by C. H. Aldrich to include particle beam injection and by D. W. Forslund to include aperiodic boundary conditions in the y-direction, to conform closely to the ANSI FORTRAN 77 standard, and to function on the UNIX operating system. Assembly language particle movers have been written by L. E. Rudsinski to maximize code performance on the CRAY-1 computer. The code has been run under 7 different operating systems in

the past decade.

A preliminary input parameter list has been constructed and run-time requirements for potentially useful problems are being considered. Because it is possible to overcommit our hours or computer time with such a code, we give more immediate priority to improved modeling with the pre-existing 1-D electrostatic code; under our first year effort we have devoted most of our small computational effort to preparing 1-D code modeling.

But the radial boundedness of the electron beam is expected to lead to jetting of the plasma ions, and the stability or overstability of the radial ion motion cannot yet be predicted. Radial oscillations could lead to the emission of clearly defined bunches just as easily as axial space-charge oscillations, and the size (and energy content) of the bunches would likely be controlled by the frequency (etc.) of the oscillations. Hence we see 2-D modeling as potentially quite important to understanding bunching.

The WAVE code is a relatively small code which spends most of its time in just a few small subroutines. This makes it relatively easy to optimize for particular machines and to understand how it works. The code uses finite sized particles to represent the electrons and ions and solves Maxwell's equations on a finite grid using the sources of charge and current from the particles. At each time step these fields are used to advance the particles and the process is repeated.

The subroutine TRANS obtains the particles from disk through a multichannel triple buffered disk input-output module. The batches of particles are brought in from disk and sent to one of three particle moving routines depending on the selected physics and to the diagnostic

routine PDIAG for either movie or still frame diagnostics at the appropriate time. The batch is then returned to disk through the I/O buffer. If the maximum number of particles will fit into the I/O buffer, the particles are never transferred to disk. After processing all the particles, the electromagnetic fields are advanced to the next time level using the updated sources of charge density and current density. Finally, at selected time steps the DIAGNOS routine is called to provide graphical output of the grid quantities. A variety of input controls of these diagnostics are available.

The code requires a spatial mesh size small compared with c/ω_p and timesteps a small fraction of the local plasma period. As a result, its use for macroscopic or long-timescale dynamics is likely to be prohibitively expensive. We expect it to be useful as a tool to simulate 2-D behavior of space-charge oscillations in the source plasma sheath region, and perhaps the dynamics of low-density background plasma surrounding a denser plasma blob.

4. SOURCE PLASMA

In order to coordinate closely with the concurrent experimental efforts, we analyze first the ionization processes in the ~ 2 cm gas puff ($P \leq .1$ torr) through which the electron beam (described above) propagates and from which it extracts ions to form a partially neutralized propagating plasmoid downstream. As a first approximation in describing the electron and ion density buildup by ionization, we ignore the effects of electric fields inside the ionizing gas puff. The gas, puffed transversely across the electron beam path adjacent to the Luce diode, is exposed to beam electrons and cathode radiation through the anode aperture, approximately 1 cm in diameter.

We calculate and compare (a) impact ionization by the 1 MeV reflexing electron beam, and (b) photoionization by cathode UV radiation. The beam is modeled as a density $n_b(t)$ given, for the first 10 ns, by

$$n_b(t) = 10^{10}\text{cm}^{-3} \cdot (t/10\ \text{ns}) \ .$$

Assuming the beam has spread radially to 1 cm diameter, this corresponds to a peak one-way current of 33 kA for a radially flat beam profile. For H_2, we expect this primary ionization to build plasma density according to

$$\dot{n}_e = 6.8 \times 10^8\text{cm}^{-3}/\text{ns}\ \left(\frac{P}{0.1\ \text{torr}}\right)\left(\frac{t}{10\ \text{ns}}\right)\left(\frac{n_{bmax}}{10^{10}\text{cm}^{-3}}\right)$$

i.e.,

$$n_e(\text{cm}^{-3}) \sim 3.4 \times 10^9\left(\frac{P}{0.1\ \text{torr}}\right)\left(\frac{n_{bmax}}{10^{10}\text{cm}^{-3}}\right)\left(\frac{t}{10\ \text{ns}}\right)^2 \ .$$

To estimate the photoionization rate, we suppose the cathode plasma to be a blackbody radiating as a 7 eV plasma. The radiation flux over a 2π hemisphere solid angle, from the 15 mm radius cathode (.0707 cm^2), with unit emissivity, would be

$$P(w) = 1.7 \times 10^7 \left(\frac{T_c}{7\ eV}\right)^4 ,$$

with a more or less uniform radiation intensity a distance r (cm) from the cathode center,

$$I_\phi (W/cm^2) \approx 2.7 \times 10^6 \left(\frac{T_c}{7\ eV}\right)^4 \frac{1}{r^2_{cm}}$$

The H_2 photoionization cross-section rises quickly from the 13.6 eV photon-energy threshold to peak at $\sigma_{\phi i} \approx 10$ Mbarns $= 10^{-17} cm^2$ (Fig. 4). The integrated radiation intensity above 14 eV from a 7 eV blackbody is about 80% of the total flux, so we multiply I_ϕ by 0.8 and use the peak cross-section. This gives

$$n_e (cm^{-3}) \sim \frac{2.3 \times 10^{14}}{r^2\ (cm^2)} \left(\frac{P}{0.1\ torr}\right)\left(\frac{t}{10\ ns}\right)\left(\frac{T_c}{7\ eV}\right)^{\sim 4}$$

for constant cathode conditions during the first 10 ns. (This corresponds to about 6.5% ionization of the gas, increasing to ~20% by 30 ns when the beam stops.)

Thus we conclude that, even if the emissivity of the cathode is as low as 0.1 and its temperature as low as 3.5 eV instead of 7 eV, photoionization probably dominates over impact ionization by the 1 MeV beam electrons. This is an important departure in the group's modeling

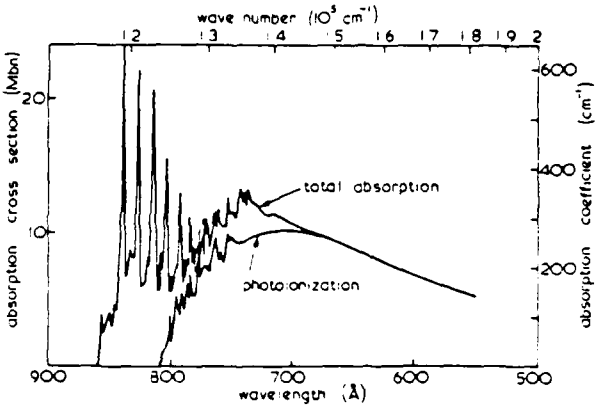

FIG. 4. Absorption cross-sectional plots for molecular hydrogen based on Cook and Metzger (1964a).

of the ion-source plasma formation.

The modeling of avalanche ionization in the electric fields of the rising beam has not yet been included. The radial space-charge electric field, E_r, of a .5 cm-radius beam with $n_b = 10^{10}cm^{-3}(t/10\ ns)$ is of order 4 MV/cm • (t/10 ns) at the beam edge, if there is no space-charge neutralization. But in about 1 ps, photoionization can produce $n_p \sim n_b$, so that if the initial plasma electrons are expelled by the fields, charge neutralization is established very early and no such radial field magnitudes build up. Likewise, inductive fields due to the rise of net current are much reduced by the return current carried by photoionized electrons. Since our model predicts $n_p/n_b \gtrsim 10^4$ at all times, these return currents probably do not greatly modify the plasma otherwise.

With the preceding model, the ratio of beam density to plasma density is nearly constant during the beam rise phase

$$\frac{n_b}{n_p} \sim 10^{-4} .$$

For $n_b/n_p = 10^{-4}$ and $n_p \sim 10^{14}(t/10\ ns)$, one has

$$\left(\frac{n_b}{n_p}\right)^{1/3} \omega_p \approx 2.6 \times 10^{10}\left(\frac{t}{10\ ns}\right)^{1/2}\left(\frac{P}{0.1\ torr}\right)^{1/6} .$$

If plasma density gradients do not interfere, this means a growth rate of the hydrodynamic electron-electron two-stream instability on the order of

$$\gamma(sec^{-1}) \sim 10^{10}\left(\frac{t}{10\ ns}\right)^{1/2}\left(\frac{P}{0.1\ torr}\right)^{1/6} ;$$

(at t ≈ 10 ns, the beam moves 2.6 cm in one growth time, and so traverses

the plasma in about one e-folding time of the unstable space-charge oscillations.) The frequency of the unstable waves is

$$f_p = \frac{\omega_p}{2\pi} \sim 0.9 \times 10^{11} \left(\frac{t}{10\ \text{ns}}\right)^{1/2} \left(\frac{P}{0.1\ \text{torr}}\right)^{1/2} ,$$

which should be detectible by its conversion to EM waves at this frequency of order 90 GHz. The 10 ns beam-rise time represents 3650 or so plasma oscillation periods (their variation included), or some 67 growth times, and one may thus expect a fully-developed two-stream instability in the source plasma unless gradients significantly damp the instability. (The plasma is only about 20 wavelengths thick, at the most unstable wavelength.)

Such a microinstability, if it exists, probably has two important effects besides generation of microwave diagnostic radiation: it can make the plasma electrons effectively more collisional and less tied to magnetic field lines, and it can spread the energy distribution of the beam electrons. The latter may already be observed, in the large beam temperatures required for consistency with the observed downstream beam equilibrium, and the former may also be observable.

The photoionization of the 10^{-5} torr "vacuum" region of the Maryland experiment may also provide a space-like low-density ambient plasma through which the fast electrons and accompanying ions propagate downstream. Here, according to the propagation stability analysis of Sec. 5, the growth rate in the beam frame should be of order

$$\left[\frac{n_e(\text{vac})}{n_b}\right]^{1/3} \omega_{pb} \sim 10^{10} [r(\text{cm})]^{-5/3} \left(\frac{t}{10\ \text{ns}}\right)^{1/2} \left(\frac{T_c}{7\ \text{eV}}\right)^{4/3} ,$$

or less if the beam is now "hot". At 3 to 10 cm from the cathode with full emissivity, this growth rate would vary from 10^9 to $10^8 s^{-1}$ at t = 10 ns, and would have a signature of microwave emission at and below 1.3 GHz if present. This growth rate corresponds to .25 to 2.5 m of beam travel, and, since the beam only traverses about 1 m in the experiment, significant exponentiation probably cannot be seen.

5. STABILITY OF PROPAGATING PLASMOID - LINEAR THEORY

The first step in the theoretical analysis of plasmoid propagation is to evaluate the stability, (or growth rates, if unstable), of a quasi-neutral beam passing through a tenuous quasi-neutral plasma. This is done by treating the background plasma as a perturbation on the beam, in the beam frame; i.e., reversing the usual roles of beam and plasma.

Even before a mostly force-neutralized plasmoid is 'disconnected' from its source, streaming instability may affect its momentum scatter, if the instability grows fast enough (i.e., in a time much less than the plasmoid length divided by the front velocity). But, for sufficiently tenuous background, the most important instability effects may be seen only on a longer timescale, once the plasmoid is propagating freely. This instability amplitude is enhanced by any modulations in density that may have come about during plasmoid formation and early history. Seen in the plasmoid ion (and electron) frame, the tenuous background streams by axially at relativistic speed and causes the unstable growth of density modulations (in both plasmoid and background). Depending on the absolute or convective nature of the instability in the plasmoid frame (Bers and Ram, 1982), and on the group velocity of the perturbations in that frame, these density modulations may pile up or may propagate to the rear of the plasmoid (Kuzelev and Rukhadze, 1979). In the latter case, if the growth time is not much shorter than the convection time, the unstable wave energy is shed into the background behind the plasmoid, and the plasmoid propagation may be only weakly affected by the fields of the instability.

On the other hand, if the instability grows faster than it convects to the rear of the plasmoid, nonlinear processes probably set in which

STABILITY - 1D Electrostatic, Linear Theory

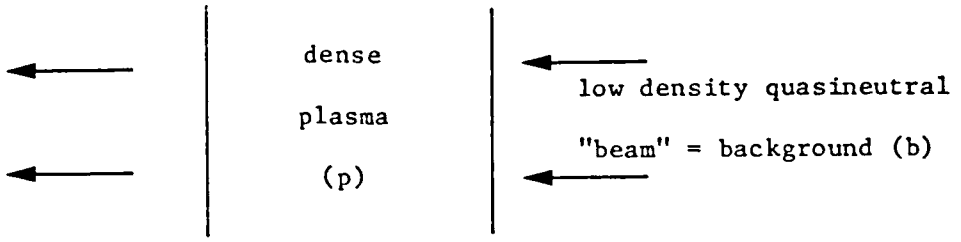

view in plasmoid frame

- High frequency mode:

$$\frac{\omega_p^2}{\omega^2} + \frac{\omega_b^2}{(\omega - \kappa \cdot v_b)^2} = 1 \qquad \text{(1D, ES)}$$

- Max $\quad \mathrm{Im}\omega \sim \left(\frac{n_b}{n_p}\right)^{1/3} \omega_p F(T_b, T_p, \ldots) \qquad$ for real k

$$\text{or } \mathrm{Im}\kappa \sim \mathrm{Im}\,\omega\,(k_{real})/v_b \sim \frac{v_{Th}}{v_b}\left(\frac{n_b}{n_p}\right)^{1/3} F(T_b, T_p)\,\lambda_D^{-1}$$

FIG. 5. Schematic of 1D, ES model and growth rate results.

lead to quasi-stationary density modulations (cavitons) in the plasmoid frame (Zakharov, 1972). It is likely that these axial dependences of density do not break up the plasmoid, but they affect the electron scattering. The issues (or two important issues) for long-range propagation of such neutralized beams are (a) what is the time required for transverse momentum spread, and (b) what is the timescale on which electrons (or ions) scattered out of the beam are replaced with accelerated background particles (because this determines not only an energy loss rate, but also a residual set of electric and magnetic fields). The presence of instability microfields impacts both of these issues.

In addition to the conventional streaming instability of space charge bunching, there is a purely electromagnetic filamentation instability (Benford, 1973) which can strongly enhance the rate of transfer from parallel to transverse momentum. For very energetic beams in axial magnetic guide fields this instability can grow even faster than the electron-electron two-stream (Ottinger and Guillory, 1979), although for moderate-gamma beams it is more slowly growing. Even if this mode is considerably slower than two-stream modulation growth, it may affect the transverse beam spread more, because of the transverse nature of the unstable fields and the different wave convection rate along the beam. We have not treated this filamentation mode in our first-year effort, but have turned our attention to the electron-electron two-stream interaction discussed above. The 1D ES model is shown in Fig. 5 and the main results from this initial analytical investigation are tabulated.

6. STABILITY OF PROPAGATING PLASMOID - NONLINEAR THEORY

Computer simulation of the nonlinear stage of electron-electron two-stream instability in a bounded system with the beam exit boundary "free" have been ongoing in the University's Space Sciences Laboratory under NSF funding and were made available without charge to this contract. We report here some of the results of those simulations by H. Rowland.

A 1-D electrostatic particle-in-cell code was run with a warm tenuous 'beam' (b) entering from the left of a region of initially-uniform, equally warm plasma (p). In the run shown here, loss of plasma particles to the boundaries was compensated by injection of Maxwellian plasma from the right-hand boundary, and injection of 'beam' plus Maxwellian distribution from the left. The right-hand boundary potential was allowed to float. The ratio of densities n_b/n_p for the run shown was 0.02.

The code was run both with fixed (infinitely massive) ions and with $m_i/m_e = 100$ and $T_i = T_e$. By about $600\ \omega_p^{-1}$ a relatively stationary soliton of width 30-40 λ_D was observed at $x = 180\ \lambda_D$ from the injection side. Its amplitude was about 3 1/2 times larger with mobile ions than with fixed ions. Both cases are shown in Figs. 6a and 6b at $t = 650\ \omega_p^{-1}$. Vertical units are arbitrary (i.e., not normalized) and the vertical scale is proportional to $E^2/8\pi$.

With $m_i/m_e = 100$, the field tended to accelerate some plasma electrons antiparallel to the beam direction, as shown by the logarithmic plot of the parallel velocity distribution (b+p) at $650\ \omega_p^{-1}$ in Fig. 6b. The flux of suprathermal electrons at the boundary tended to have an erratic spiky time history. These results were presented by Rowland at

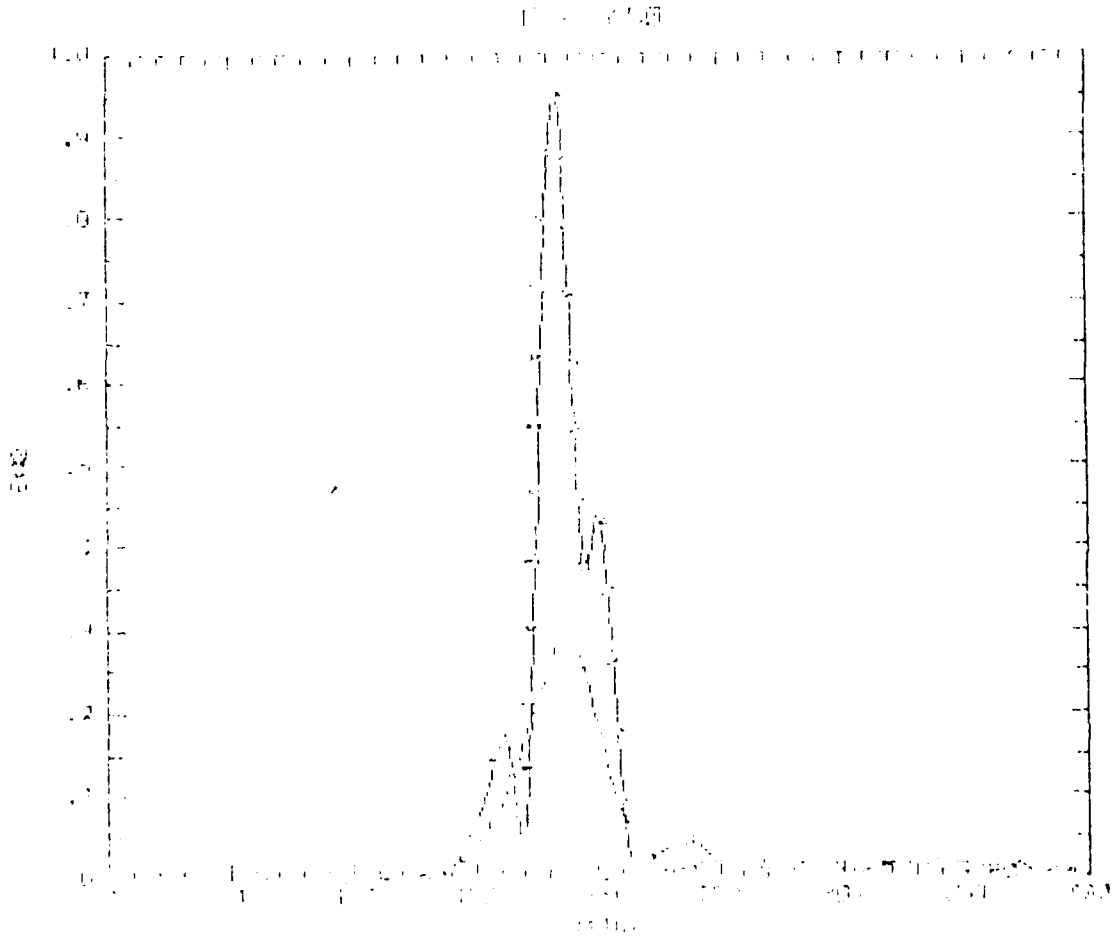

FIG. 6a. 1D, ES simulation with $m_i/m_e \to \infty$. $t = 600\ \omega_p^{-1}$.

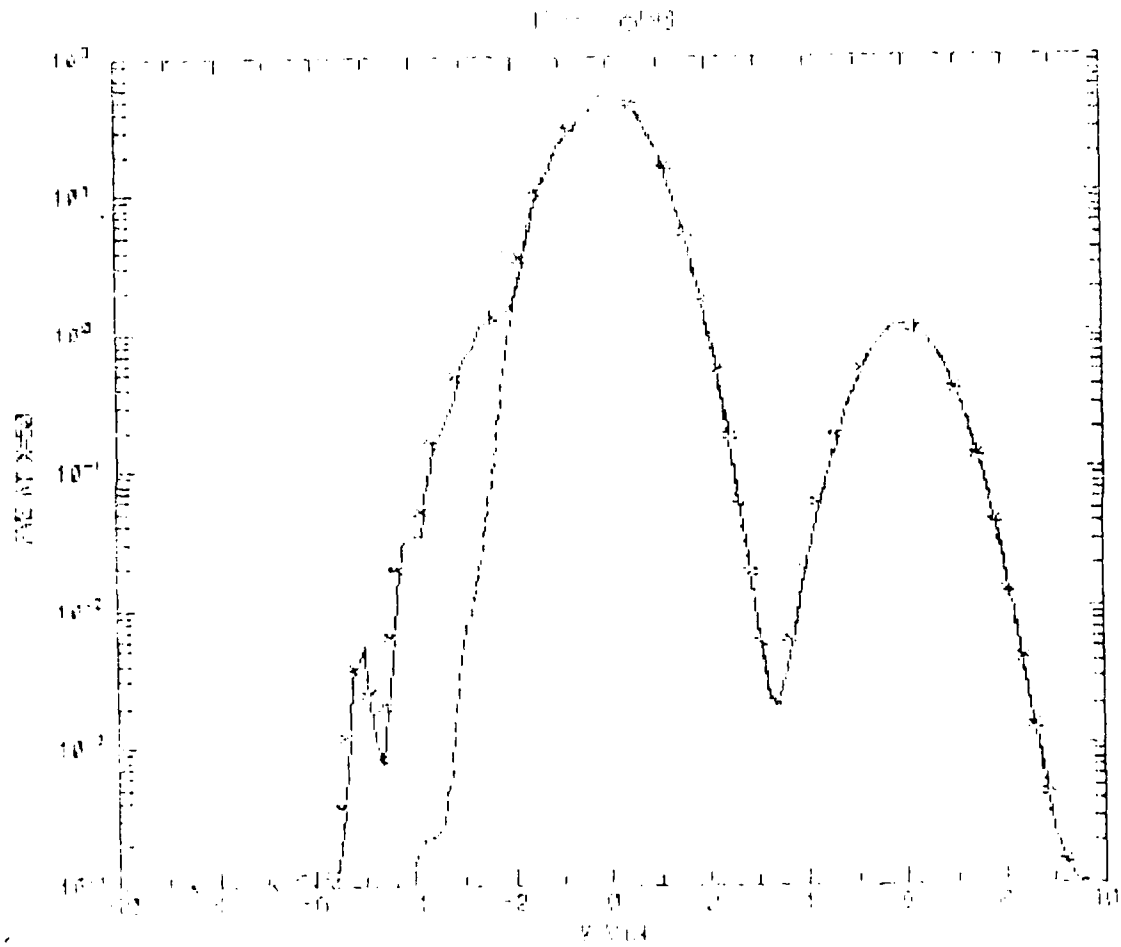

FIG. 6b. 1D ES simulation with $m_i/m_e = 100$. $t = 600\ \omega_p^{-1}$.

the AGU meeting in Baltimore in May 1986 and further studies were described at the November 1986 APS-DPP meeting.

We have suggested further runs of this code with a cold beam and with modified plasma particle boundary conditions.

Calculations of the peak electrostatic oscillation energy $E_{max}^2/8\pi$, normalized to the background streaming energy in the plasmoid frame $(\gamma-1)n_b mc^2$, for $\gamma \leq 10$ (e.g., Matsiborko et al., 1971) have shown that

$$W = E_{max}^2/[8\pi n_b mc^2(\gamma-1)] \sim (\gamma+1)(n_b/n_p)^{1/3}/4\pi$$

when $\gamma(n_b/n_p)^{1/3} << 1$ and when saturation can occur inside the plasmoid.

For a background density $n_b = 10^6 cm^{-3}$, $\gamma = 2$, and $n_p = 10^{10} cm^{-3}$ as an example, one has $W = 10^{-2}$, $E^2/8\pi = 0.9 \times 10^{-2} erg/cm^3$ and $E \sim 190$ V/cm at saturation. The ponderomotive pressure in the field peak corresponds to only 7×10^{-6} torr, compared with a thermal pressure in the plasmoid frame of

$$P_{th}(torr) \sim 1.2 \times 10^{-3}\left(\frac{n_p}{10^{10} cm^{-3}}\right)\left(\frac{T_p}{100\ eV}\right) .$$

Thus we do not expect hydrodynamic disruption of the plasmoid by 'solitons' in such a low-density-background case.

But for $n_b = 10^8 cm^{-3}$ (as could be produced by photoionization of 10^{-5} torr laboratory vacuum in a drift tube), the ponderomotive pressure at saturation is about 500 times larger and is comparable to the thermal pressure in the plasmoid, leading on long-enough timescales to local expulsion, i.e., cavitation, of the plasma. The required timescales, however, would not be seen in typical drift tubes; for $\gamma = 2$, saturation

(~ 10 e-folds) f the instability requires about 6.5 meters at n_b = $10^8 cm^{-3}$, and hydrodynamic cavitation requires about 20 meters.

REFERENCES

G. Benford, "Theory of Filamentation in Relativistic Electron Beams," Plasma Phys. 15, 483 (1973).

A. Bers and A. Ram, "Relativistic Pulse Shapers of Absolute and Convective Instabilities," Bull. Am. Phys. Soc. 28, 919 (October 1982).

W. W. Destler, P. G. O'Shea, and M. Reiser, "Propagation of an Intense Relativistic Electron Beam through a Plasma Region into Vacuum," Phys. Fluids 27, 1897 (July 1984).

M. V. Kuzelev and A. A. Rukhadze, "Numerical Simulation of the Nonlinear Evolution of the Two-Stream Instability in a Bounded Plasma," Sov. Phys. Tech. Phys. 24, 654 (1979).

P. F. Ottinger and J. Guillory, "Beam-Plasma Interactions in a Filled Waveguide Immersed in an Applied Axial Magnetic Field," Phys. Fluids 22, 466 (March 1979).

S. J. Stephanakis, S. A. Goldstein, and D. Mosher, NRL Memorandum Report 4948 (September 1982).

V. K. Tripathi, P. F. Ottinger, and J. Guillory, "Thermal-Resistive Current Filamentation in the Cathode Plasma of a Pinch-Reflex Diode," J. Appl. Phys. 54, 3043 (1983).

V. E. Zakharov, "Collapse of Langmuir Waves," Sov. Phys. JETP 35, 908 (November 1972).

APPENDIX A

List of Papers or Presentations Resulting from this Work

1. W. W. Destler, R. J. Faekl, P. G. O'Shea, M. Reiser, Z. Segalov, C. D. Striffler, and X. Zhang, Beams 86, Sixth Inter. Conf. on High-Power Particle Beams, June 9-12, 1986, Kobe, Japan (attached).
2. X. Zhang and C. D. Striffler, Bull. APS 31, 1429 (1986). Poster presentation (attached).

INTENSE BEAM PROPAGATION PROPERTIES IN MAGNETIZED AND LOCALIZED ION SOURCE CONFIGURATIONS

W. W. Destler, R. J. Faehl, P. G. O'Shea, M. Reiser, Z. Segalov, C. D. Striffler, and X. Zhang
Electrical Engineering Department, University of Maryland, College Park, Maryland 20742 U.S.A.

Abstract

During the past few years we have performed both experimental and theoretical studies on the propagation of intense electron beams into an evacuated drift tube. In one set of studies the radial force balance is achieved by an applied magnetic field and in a second set of studies the radial force balance is achieved by ions that have been created in a localized region of the tube and collectively accelerated.

Introduction

In recent years, the propagation of intense relativistic electron beams (IREB's) has been the subject of many studies, in part due to their various applications in such diverse fields as high power coherent radiation source development, collective ion acceleration, and plasma heating and confinement. A summary of the field prior to 1982 is presented in the book by R. B. Miller.[1]

A schematic of the experimental system in our studies is shown in Fig. 1. The IREB is field emitted from a cathode 1.2 cm upstream of a stainless steel anode. The nominal properties of the electron beam injected into the vacuum chamber are 1 MeV, 25 kA, 30 ns FWHM. Various diagnostic equipment is employed in the experiments, one of which is the current collector/calorimeter shown in the figure. In the first set of studies discussed, a magnetic field immerses the entire system and in the second set of studies, a puff valve supplying a localized gas cloud is placed immediately after the anode. No magnetic field is applied in the latter studies.

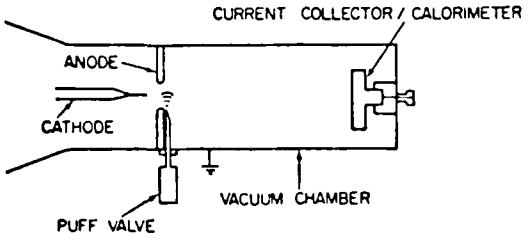

FIG. 1. Experimental configuration.

Magnetically Confined Beam Propagation

For the magnetically confined studies, the propagated current is determined as a function of the uniform applied magnetic field (0-2 T) for various drift tube diameters, cathode geometries, and anode aperture sizes.

Experiments

The experimental configuration is shown in Fig. 1 with the absence of the puff valve. A solid cathode and anode apertures of 1.2 and 2.6 cm are used in combination with stainless steel drift tubes of 3.8, 9.8, and 14.8 cm inner diameter. The beam current propagating to the end of the drift tube is measured using a low impedance current collector. The injected beam current is measured by placing the collector 2 cm downstream of the anode plane and is found to be 27 ± 1 kA independent of applied magnetic field. The vacuum maintained is in the range 10^{-5}-10^{-4} Torr.

The peak electron beam current measured at the downstream end of the 70 cm long drift tube as a function of applied magnetic field B is shown in Fig. 2 for the various geometries considered. The following important features are apparent from the measurements:

1. In all tubes there appear to be three distinct regimes of beam propagation. These distinctions are most obvious in the 14.8 and 9.8 cm diameter tube results.

(a) Low Magnetic Field. Propagating current initially rises as B is increased from zero. Here we have a poorly confined beam, a significant fraction of which may hit the tube wall. As B increases, the beam confinement improves and more current propagates.

(b) Intermediate Magnetic Field. Beam current decreases rapidly with increasing B with space-charge effects playing an increasingly significant role in this region.

(c) High Magnetic Field. A plateau region where the change in propagating current is small as B increases.

2. As tube diameter decreases, the region of maximum current propagation shifts to higher magnetic fields, and the propagating current in the high field plateau region increases.

3. For the 14.8 and 9.8 cm diameter tubes, changing the anode aperture size from 1.2 to 2.6 cm diameter did not greatly alter the propagating current. However, we note significant difference in the current characteristics for the high field region for the 3.8 cm tube. This is due to the fact that the anode diameter is a significant fraction of the tube diameter. The smaller anode hole case appears to exhibit similar features in the region $0.8 \lesssim B \lesssim 1.1$ T as the large tubes do in the range $\sim 0.3 \lesssim B \lesssim 0.5$ T. We have evidence that the current propagating in this tube for the 2.6 anode begins to decrease at B = 1.2 T and above.

The fact that the smallest tube can propagate as much current at high B as the large ones can at considerably lower B removes from consideration the possibility that some form of magnetic mirroring, resulting from nonuniformity of the applied field causes the observed reduction of current in the large tubes at high magnetic field.

Model of Solid Beam Equilibrium

A steady-state model of an IREB in an axis-symmetric system can be constructed by conserving single particle energy and canonical angular momentum, applying continuity of current, and maintaining force balance. The beam model and its various parameters are shown in Fig. 3. We assume that a solid, uniform density electron beam of radius R_1 is injected into a long grounded cylindrical drift tube of radius R_w. The injected beam is monoenergetic with energy

$$mc^2(\gamma_o - 1) = eV_o .$$

After the beam passes through the anode, it

expands adiabatically to a radius R_b where a laminar flow equilibrium is set up far from the end walls. The entire system is immersed in a uniform magnetic field B_{AZ}. The downstream beam properties are the charge density $\rho(r)$ and the azimuthal and axial velocities $V_\phi(r)$ and $V_z(r)$. The fields generated by the beam are confined inside the drift tube, and include the radial electric field $E_{sr}(r)$ and the azimuthal and axial magnetic fields $B_{s\phi}$ and B_{sz}.

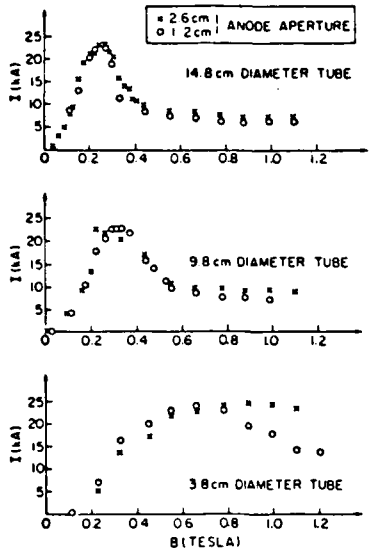

FIG. 2. Peak propagating current measured at the current collector for various drift tubes and anode apertures using a solid cathode.

To further simplify the analysis, the equilibrium beam density is assumed constant across the beam $\rho(r) = \rho_b$, allowing the electric potential $\phi(r)$ and the electric field to be easily calculated. Conservation of single particle energy gives

$$\gamma(r) = \gamma_o + \frac{e}{mc^2}\phi(r) = [1 - \beta_\phi^2(r) - \beta_z^2(r)]^{-1/2} , \tag{1}$$

where

$$\phi(r) = \frac{\rho_b R_b^2}{4\epsilon_o}\left[1 - \frac{r^2}{R_b^2} + 2\ln\left(\frac{R_w}{R_b}\right)\right] . \tag{2}$$

In a laminar flow beam of uniform density, canonical angular momentum conservation can be written as

$$\frac{eB_{AZ}r^2}{2}\left(\frac{R_a}{R_b}\right)^2 = r[m\gamma(r)V_\phi(r) - eA_\phi(r)] , \tag{3}$$

where $A_\phi(r) = rB_{AZ}/2 + A_{s\phi}(r)$ is the total azimuthal component of the magnetic vector potential. Solving Eq. (3) for $V_\phi(r)$ and substituting it into $J_\phi(r) = \rho_b V_\phi(r)$, we obtain from Maxwell's Equations an inhomogeneous differential equation for $A_{s\phi}$. This equation can be solved, from which $B_{s\phi}$ is computed, then $V_z(r)$ is calculated by Eq. (3), $V_\phi(r)$ via Eq. (1), and B_{sz} from Ampere's Law.

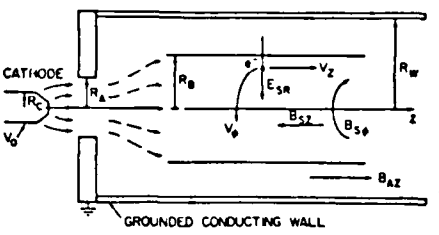

FIG. 3. Schematic of the beam model.

At this point, the functional forms of all the equilibrium beam properties have been found in terms of R_a, R_b, R_w, γ_o, B_{AZ}, and the beam density ρ_b. In addition, we require each volume element of the beam to be in radial force balance, which can be written as

$$\frac{m\gamma(r)V_\phi^2(r)}{r} = e\{E_{sr}(r) + V_\phi(r)[B_{AZ} + B_{sz}(r)] - V_z(r)B_{s\phi}(r)\} . \tag{4}$$

To solve this equation, R_a, R_b, R_w, γ_o, and B_{AZ} are held fixed while ρ_b is varied until the "best possible equilibrium" is found. After calculating the beam density for an equilibrium, the axial beam current is calculated from

$$I = 2\pi\rho_b \int_0^{R_b} V_z(r)\, r\,dr , \tag{5}$$

which equals the injected current.

From the above model, we can generate the maximum propagated current as a function of applied magnetic field B_{AZ}. A specific example is shown in Fig. 4. In the limit of large magnetic field, $R_b \to R_a$, the peak beam current agrees well with the Bogdankevich-Rukhadze limiting current[2]

$$I_{BR} = \frac{17(\gamma_o^{2/3} - 1)^{3/2}}{1 + 2\ln(R_w/R_b)} \quad [kA] \tag{6}$$

which is plotted for reference. As B_{AZ} decreases, the beam expands ($R_b > R_a$) and the peak current is limited by space charge effects. A rapid increase occurs in the region, 0.4-0.6 T, where the current is limited by total field energy. The beam fills the tube below the peak, $B_{AZ} \sim 0.3$ T, where the current is limited by the size of the tube.

In comparison, the model predicts all the experimental trends. The main disagreement is in the magnitude of the applied magnetic field. Here the theory is off by approximately a factor of two. It is expected that cyclotron motions, other nonlaminar effects, and nonadiabatic expansions will account for some of this discrepancy. A detailed description of this system is presented in Ref. 3.

Localized Ion Source Beam Propagation

For the localized ion source studies, we measure the propagated current as a function of the ion source properties. The ion source is from a localized gas cloud in the immediate vicinity of the injected electron beam (puff valve). A

virtual cathode forms in the ion source region, where the strong electric field (100-500 MV/m) is able to accelerate the ions downstream and allow the formation of a propagating beam.[4]

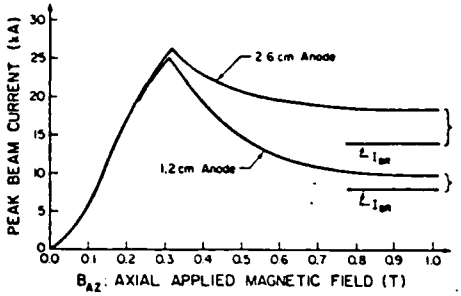

FIG. 4. Maximum beam current versus applied magnetic field for two different anode sizes. R_w = 1.9 cm, γ_o = 3.5.

Experiments

The experimental configuration is shown in Fig. 1. An IREB is emitted from a 6 mm diameter tungsten cathode. A 25 mm aperture in the anode allows almost all of the beam electrons to pass through into the downstream drift region. The drift tube diameter is 15 cm. Ions to be accelerated are produced by electron impact and ion-ion avalanche ionization[4] of the localized gas cloud. The firing of the fast gas puff valve is adjusted to ensure that the gas cloud is localized within 2-3 cm of the anode plane at the time of electron beam injection.

The diagnostics used are a number of current probes to measure both the axially propagating current and the radial current at the drift tube walls. In addition, a 7.5 cm diameter combination Faraday cup/calorimeter measures the integrated net axial beam current and energy.

Measurements of the net current propagated to a given axial position using the Faraday cup are displayed in Fig. 5(a). Shown in Fig. 5(b) is the energy deposited in the calorimeter and in Fig. 5(c) the counts from a silver activation neutron detector as a function of gas cloud pressure. When the peak pressure of the localized gas cloud is adjusted to an optimum value (about 35 mTorr), beam current many times the B-R space charge limiting value, Eq. (3), can be propagated down the drift tube. In the absence of the ion source, currents well below the space charge limit are observed. At the optimum value, a large fraction of the injected current propagates to the axial location of the Faraday cup. The range in pressure about the optimum narrows as the cup location is moved farther downstream. This appears to be limited only by the pulse duration of the injected electron beam or by the depletion of the source of ions at the injection point.

Using a radial array of axial current probes, measurements have been made of the propagating current profile. Several features are worthy of mention: (1) the current profile is virtually flat and the measured current levels are very low when no localized ion source is present, (2) the best radial confinement of the beam electrons is observed at a peak gas cloud pressure of about 35 mTorr (corresponding to the optimum pressure for peak net current propagation discussed above), and (3) a hollowing out of the beam is observed when the gas cloud pressure exceeds this optimum value.

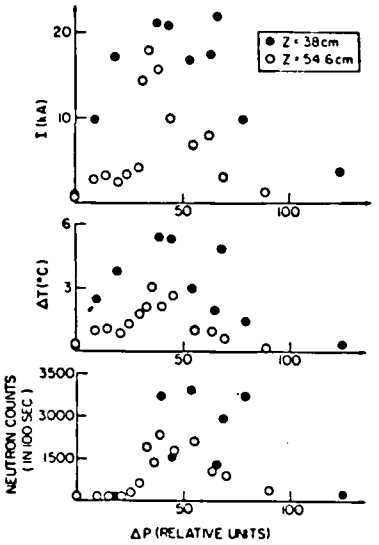

FIG. 5. Results of (a) current collector, (b) calorimeter, and (c) neutron detector measurements at two axial locations as a function of gas-cloud peak pressure (p_{max}).

An axial array of wall probes installed to measure the radial current flowing to the walls has resulted in considerable insight. Several features are again worthy of note: (1) with no localized ion source at the injection point, the wall currents are quite high at the injection end and fall off to very low values as the probe axial position is increased; (2) for the probe closest to the injection point the observed current is lowest at a peak pressure of about 30 mTorr, the same pressure at which the high downstream wall currents are observed; and (3) gas cloud pressures above the optimum result in higher wall currents at the injection end. These as well as a more extensive presentation of the experimental studies appear in Refs. 5 and 6.

Model of Electron-Ion Beam Equilibrium

A steady-state electron-ion beam model is formulated that relates the downstream equilibrium parameters to the initial injection properties of the system. Because there is no applied magnetic field, the propagation depends on the presence of ions which come from a localized source near the entrance end of the injected beam. The electron beam is assumed to have a transverse temperature T_e in addition to its axial velocity and the ions have only an axial velocity. A schematic of the model is shown in Fig. 6. An electron beam of kinetic energy $mc^2(\gamma_o - 1) = eV_o$ and current I is injected into a long cylindrical drift tube of radius R_w. The ion source parameters are a formation rate S_i (C/sec) in a potential V_i (V). As shown, the system evolves into a downstream equilibrium that contains both ions and electrons with axial velocity of $v_i = \beta_i c$ and $v_e = \beta_e c$, respectively, in a potential $\bar{V}$. The system in general possesses a net charge and net current.

The downstream equilibrium of the ions and electrons requires radial force balance which

results in a radial density profile for the electrons and ions of

$$n_e(r) = \frac{n_o}{[1 + (r/a)^2]^2} = \frac{1 - \beta_{zi}^2}{1 - \beta_{zi}\beta_{ze}} n_i(r) \quad (7)$$

where

$$n_o = \frac{8\varepsilon_o kT_e}{e^2 a^2} \frac{1 - \beta_{zi}^2}{(\beta_{ze} - \beta_{zi})^2} . \quad (8)$$

This profile is characterized by a peak density n_o and an effective radius "a." Continuity of current for each species gives

$$I_o = \frac{8\pi\varepsilon_o ckT_e}{e} \frac{\beta_{ze}(1 - \beta_{zi}^2)}{(\beta_{ze} - \beta_{zi})^2} \quad (9)$$

$$S_i = \frac{8\pi\varepsilon_o ckT_e}{e} \frac{\beta_{zi}(1 - \beta_{zi}\beta_{ze})}{(\beta_{ze} - \beta_{zi})^2} . \quad (10)$$

Conservation of energy gives

$$\gamma_e = \gamma_o + \frac{eV}{m_e c^2} = \frac{1}{(1 - \beta_{ie}^2 - \beta_{ze}^2)^{1/2}} \quad (11)$$

$$\gamma_i = 1 + \frac{eV_{io}}{m_i c^2} - \frac{eV}{m_i c^2} = \frac{1}{(1 - \beta_{zi}^2)^{1/2}} \quad (12)$$

where $\beta_{ie}^2 = kT_e/m_e c^2$. The on-axis downstream potential is

$$V(0) \equiv V = -\frac{2kT_e}{e} \frac{\beta_{zi}}{\beta_{ze} - \beta_{zi}} \ln[1 + (\frac{R_w}{a})^2] \quad (13)$$

and the net current can be calculated from $I_{net} = S_i - I_o$.

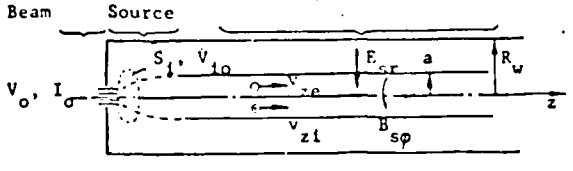

FIG. 6. Schematic of the model.

The above model is analyzed for the case I_o = 25 kA, eV_o = 1 MV, and R_w/a = 10. An electron beam temperature is chosen and then the above equations are solved for β_{ze}, β_{zi}, V, V_{io}, and S_i. These results are shown in Fig. 7 where we have plotted normalized net current versus electron beam temperature. The regime of interest to us is where I_{net}/I_o is near - 1. When it is exactly - 1, $T_e = T_e^* \approx 240$ keV and $\beta_{zi} = 0$. That is, the system is charge neutralized and represents the traditional Bennett equilibrium. The regime in temperatures just below T_e^*, 200 keV $\lesssim T_e < T_e^* \approx 240$ keV, gives rise to a system that is almost charge neutralized [$f \equiv n_i/n_e \gtrsim 0.96$], the ion source rate is small [$S_i/I_o \lesssim 0.10$], the ion potential at the source is small [$V_{io}/V_o \lesssim 2.0$ going to zero at T_e^*], and the ion axial velocity $\beta_{zi} \lesssim 0.07$. These results are in good agreement with the experimental results and the source rate S_i is in excellent agreement with ionization rates for the localized neutral gas source.

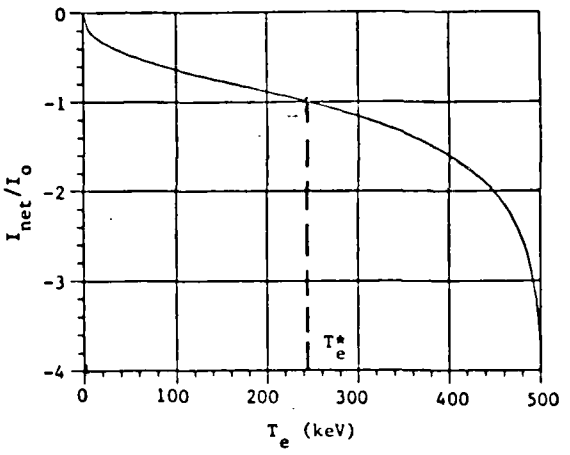

FIG. 7. Normalized net current versus electron beam temperature. The system parameters are; I_o = 25 kA, eV_o = 1 MV, and R_w/a = 10.

Summary

We have performed both experimental and theoretical studies on the beam propagation characteristics of two systems, one possessing a magnetic guide force and the other an ion guide force. Each system contains a regime where a substantial portion of the injected electron current is able to propagate to distances far from the injection end. This current is much larger than the B-R space charge limited current.[2] Our theoretical models agree well with the experimental observations not only in a qualitative sense but for many system variations, in a quantitative sense.

Acknowledgments

This work is supported by the U.S. Air Force Office of Scientific Research and the U.S. Department of Energy.

References

1. R. B. Miller, An Introduction to the Physics of Intense Charged Particle Beams, (Plenum, New York, 1982).
2. L. S. Bogdankevich and A. A. Rukhadze, Usp. Fiz. Nauk. 103, 609 (1971) [Sov. Phys. Usp. 14, 163 (1971)].
3. P. G. O'Shea, D. Welsh, W. W. Destler, and C. D. Striffler, J. Appl. Phys. 55, 3934 (1984).
4. H. Dantsker, L. E. Floyd, and C. D. Striffler, Bull. Am. Phys. Soc. 29, 1353 (1984).
5. W. W. Destler, P. G. O'Shea, and M. Reiser, Phys. Rev. Lett. 52, 1978 (1984); Phys. Fluids 22, 1897 (1984).
6. W. W. Destler, P. G. O'Shea, and Z. Segalov, IEEE Trans. Nucl. Sci. NS-32, 3481 (1985).

ANALYTIC MODEL OF INTENSE BEAM PROPAGATION THROUGH A LOCALIZED SOURCE OF IONS INTO VACUUM.* X. ZHANG AND C. D. STRIFFLER, UNIVERSITY OF MARYLAND.--A MODEL OF THE PROPAGATION OF AN INTENSE RELATIVISTIC ELECTRON BEAM INTO VACUUM AFTER PASSAGE THROUGH A LOCALIZED PLASMA HAS BEEN PREVIOUSLY PRESENTED.[1,2] IT INVOLVES A STEADY-STATE SYSTEM COMPOSED OF ELECTRONS WITH FINITE TRANSVERSE TEMPERATURE AND COLD CO-MOVING IONS. DOWNSTREAM RADIAL FORCE BALANCE, CONSERVATION OF ENERGY, AND CONTINUITY OF CURRENT LED TO RESULTS FROM THIS MODEL THAT AGREE WELL WITH EXPERIMENTAL OBSERVATIONS.[2] IN THIS PAPER, WE PRESENT RESULTS OF THE MODEL THAT INCLUDE REALISTIC PULSE SHAPES, FINITE TRANSIENT TIMES, AND LIMITATIONS ON ION FORMATION RATE DUE TO GAS CLOUD PARAMETERS. IN ADDITION, NEW VERSIONS OF THE MODEL ARE PRESENTED AND ANALYZED.

*THIS WORK IS SUPPORTED BY AFOSR AND DOE.

[1]Z. SEGALOV, ET AL., BULL. AM. PHYS. SOC. 30, 1505 (1985).

[2]W. W. DESTLER, ET AL., SIXTH INT. CONF. ON HIGH-POWER PARTICLE BEAMS, JUNE 9-12, 1986, KOBE, JAPAN.

REFERENCES

1. R. B. Miller, "An Introduction to the Physics of Intense Charged Particle Beam", (Plenum, New York, 1982)

2. R. J. Faehl, X-8, LANL, memorandum, Nov. 21, (1983)

3. W. W. Destler, et al, Phys. Rev. Lett. 52, (1984)

4. H. Dantsker, et al, Bull. APS 29, 1353 (1984)

5. Z. Segalov, et al.,Bull. APS 30, 1505 (1985)

6. W. W. Destler, et al., Sixth Int. Conf. on High-Power Partical Beams, June 9-12, 1986, Kobe, Japan.

OUTLINE

I. Introduction

II. Analysis a) Radial Force Balance

b) Continuity of Current

c) Conservation of Energy

III. Results a) $T_i = 0$

b) $T_i \neq 0$

IV. Application to Realistic Pulse Shape

V. Conclusions

A Steady-State Beam Propagation Model for an Electron Beam Injected through a Localized Plasma System

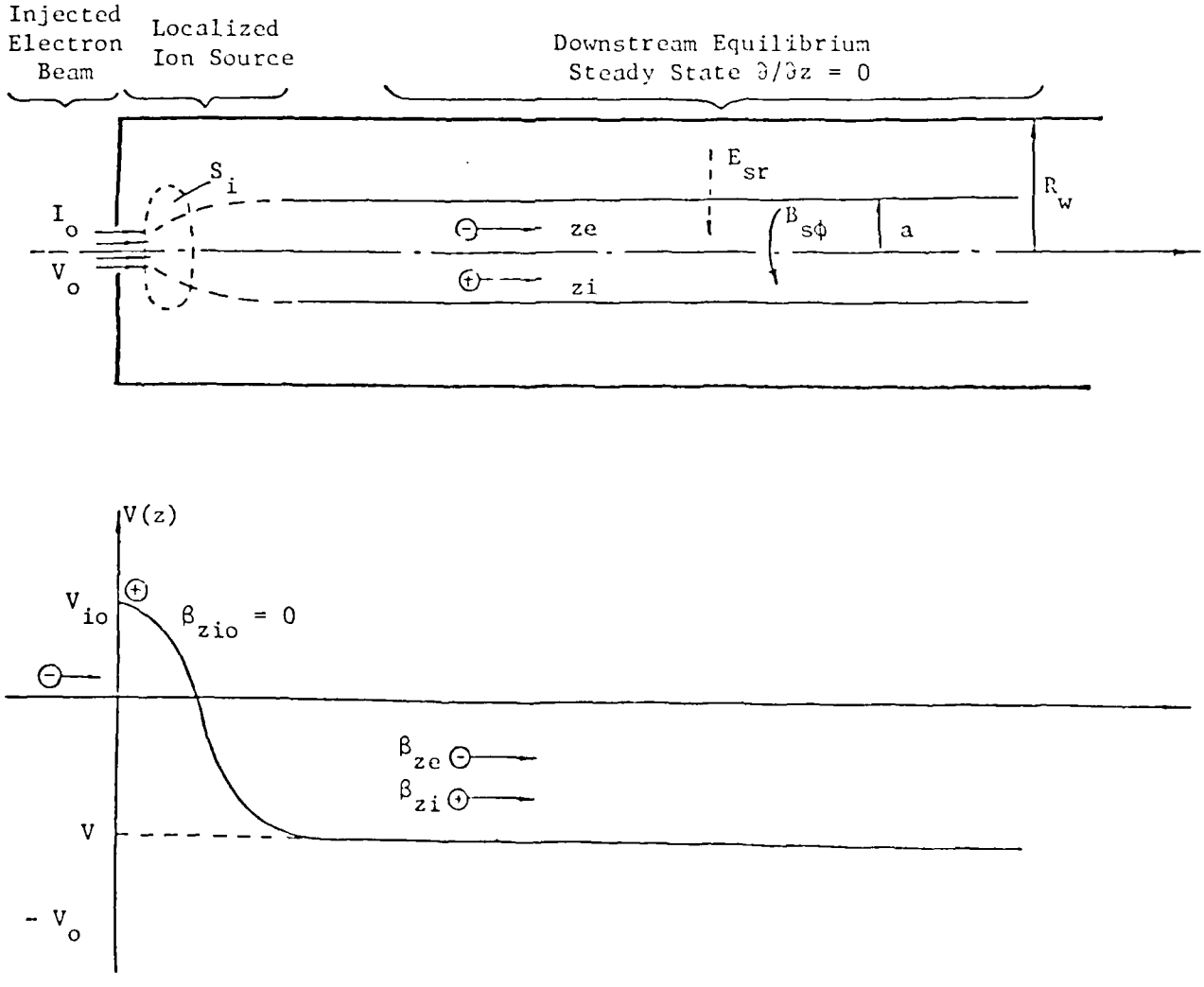

ANALYSIS

1. Downstream Equilibrium----Radial Force Balance

Equations:

$$ions: \quad ez_i n_i (E_{sr} - v_{zi} B_{s\phi}) - KT_i \frac{dn_i(r)}{dr} = 0$$

$$electrons: \quad -en_e (E_{sr} - v_{ze} B_{s\phi}) - KT_e \frac{dn_e(r)}{dr} = 0$$

where

$$E_{sr}(r) = \frac{e}{\epsilon_0 r} \int_0^r (z_i n_i(\hat{r}) - n_e(\hat{r}))\hat{r}\, d\hat{r}$$

$$B_{s\phi}(r) = \frac{\mu_0 e}{r} \int_0^r (z_i n_i(\hat{r}) v_{zi} - n_e(\hat{r}) v_{ze})\hat{r}\, d\hat{r}$$

T_i, T_e ——*transverse temperature of ion and electron.*

Solutions :

$$z_i\, n_i(r) \;=\; \frac{z_i\, n_{i\,0}}{[1 \;+\; (\frac{r}{a})^2]^2}$$

$$n_e(r) \;=\; \frac{n_{e\,0}}{[1 \;+\; (\frac{r}{a})^2]^2}$$

$$z_i\, n_{i\,0} = \frac{8\epsilon_0 KT_e}{e^2 a^2}\frac{1 \;-\; \beta_{zi}\,\beta_{ze}}{(\beta_{ze} \;-\; \beta_{zi})^2} \;+\; \frac{8\epsilon_0 KT_i}{e^2 a^2}\frac{1 \;-\; \beta_{ze}^2}{(\beta_{ze} \;-\; \beta_{zi})^2}$$

$$n_{e\,0} = \frac{8\epsilon_0 KT_e}{e^2 a^2}\frac{1 \;-\; \beta_{zi}^2}{(\beta_{ze} \;-\; \beta_{zi})^2} \;+\; \frac{8\epsilon_0 KT_i}{e^2 a^2}\frac{1 \;-\; \beta_{zi}\,\beta_{ze}}{(\beta_{ze} \;-\; \beta_{zi})^2}$$

2. Continuity of Current

Equations :

$$\textit{ions}: \quad S_i \;=\; \int e z_i\, n_i(r)\, v_{zi}\; ds \;=\; 2\pi c c\, \beta_{zi} \int_0^{R_w} z_i\, n_i(r)\, r\; dr$$

$$\textit{electrons}: \quad I_0 \;=\; \int e n_e(r)\, v_{ze}\; ds \;=\; 2\pi c c\, \beta_{ze} \int_0^{R_w} n_e(r)\, r\; dr$$

using the results of force balance, obtain:

$$I_0 = \frac{8\pi\epsilon_0 c\,\beta_{ze}}{(\beta_{ze} - \beta_{zi})^2}\left[\frac{KT_e}{e}(1 - \beta_{zi}^2) + \frac{KT_i}{e}(1 - \beta_{zi}\beta_{ze})\right]\frac{(\frac{R_w}{a})^2}{1 + (\frac{R_w}{a})^2}$$

$$S_i = \frac{8\pi\epsilon_0 c\,\beta_{zi}}{(\beta_{ze} - \beta_{zi})^2}\left[\frac{KT_e}{e}(1 - \beta_{ze}\beta_{zi}) + \frac{KT_i}{e}(1 - \beta_{ze}^2)\right]\frac{(\frac{R_w}{a})^2}{1 + (\frac{R_w}{a})^2}$$

3. Conservation of Energy

Equations:

$$\textit{ions:}\quad \gamma_i = 1 + \frac{eV_{i0}}{m_i c^2} - \frac{eV}{m_i c^2} = \frac{1}{\sqrt{1 - \beta_{zi}^2 - \beta_{ti}^2}}$$

$$\textit{electrons:}\quad \gamma_e = \gamma_0 + \frac{eV}{m_e c^2} = \frac{1}{\sqrt{1 - \beta_{ze}^2 - \beta_{te}^2}}$$

where

$$\gamma_0 = 1 + \frac{eV_0}{m_c c^2},\quad \beta_{tc}^2 = \frac{2KT_e}{m_e c^2},\quad \beta_{ti}^2 = \frac{2KT_i}{m_i c^2}$$

$$V(0) = -\int_{R_w}^{0} E_{sr}(r)\,dr = -\frac{2}{\beta_{ze} - \beta_{zi}}\left(\frac{KT_e}{e}\beta_{zi} + \frac{KT_i}{e}\beta_{ze}\right)\log_e\left(1 + \frac{R_w^2}{a^2}\right)$$

Solution Procedure

Given $I_0, V_0, \frac{R_w}{a}, T_e$ and T_i, *can solve* for $\beta_{ze}, \beta_{zi}, S_i$ and V_{io}, *can also compute* I_{net} and f.

$$I_{net} = \int_0^{R_w} 2\pi c\,(z_i n_i v_{zi} - n_e v_{ze})\,dr$$

$$= \frac{8\pi\epsilon_0 c}{(\beta_{zi} - \beta_{ze})} \frac{\frac{R_w^2}{a^2}}{1 + \frac{R_w^2}{a^2}} \left(\frac{KT_e}{e} + \frac{KT_i}{e}\right)$$

$$f = \frac{z_i n_i}{n_e} = \frac{(1 - \beta_{ze}^2)T_i + (1 - \beta_{ze}\beta_{zi})T_e}{(1 - \beta_{ze}\beta_{zi})T_i + (1 - \beta_{zi}^2)T_e}$$

Single Electron Motion in Electric-Magnetic Field Generated by Fluid

Motion equations:

$$\frac{dp_r}{dt} = m\gamma\dot{v}_r + m\dot{\gamma}v_r = -e(E_r - v_z B_\phi)$$

$$\frac{dp_z}{dt} = m\gamma\dot{v}_z + m\dot{\gamma}v_z = -ev_r B_\phi$$

where

$$\dot{\gamma} = -\frac{e}{mc^2}E_r v_r$$

$$E_r(r) = -\frac{4KT_e}{e}\frac{\beta_{zi}}{\beta_{ze} - \beta_{zi}}\frac{r}{a^2 + r^2}$$

$$B_\phi(r) = -\frac{4KT_e}{ec}\frac{1}{\beta_{ze} - \beta_{zi}}\frac{r}{a^2 + r^2}$$

and *potential*

$$V(r) = \frac{2KT_e}{e}\frac{\beta_{zi}}{\beta_{ze} - \beta_{zi}}\log_e\left(\frac{a^2 + R_w^2}{a^2 + r^2}\right)$$

Let $r = r_0 + r_1$. If one linearizes these equations about r_0, and assumes $r_1 \ll a$, he arrives at a solution with a single frequency of oscillation which depends on r_0. However, the amplitude of the displacement, r_{1max} is $> a$. This means the magnetic field is too weak to confine the electron motion inside the beam radius if only taken to linear order. Therefore, we must keep high order terms.

Equilibrium Results ($T_i = 0$)

$T_i = 0 \quad V_0 = 1.0\ MV \quad \frac{R_w}{a} = 10$

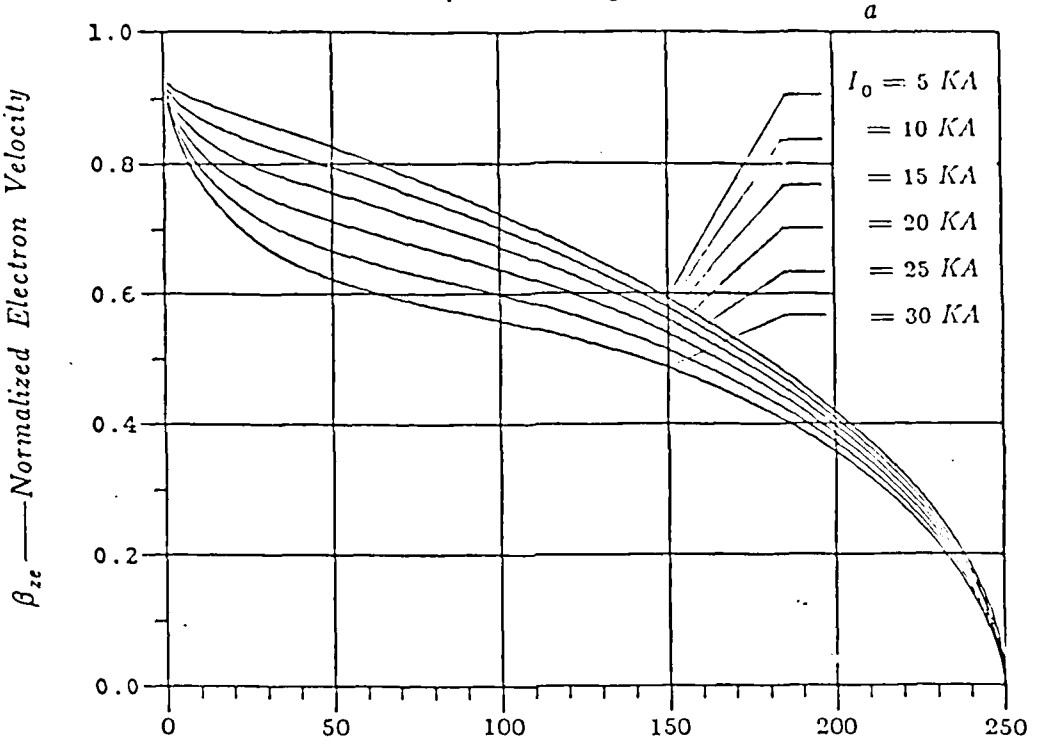

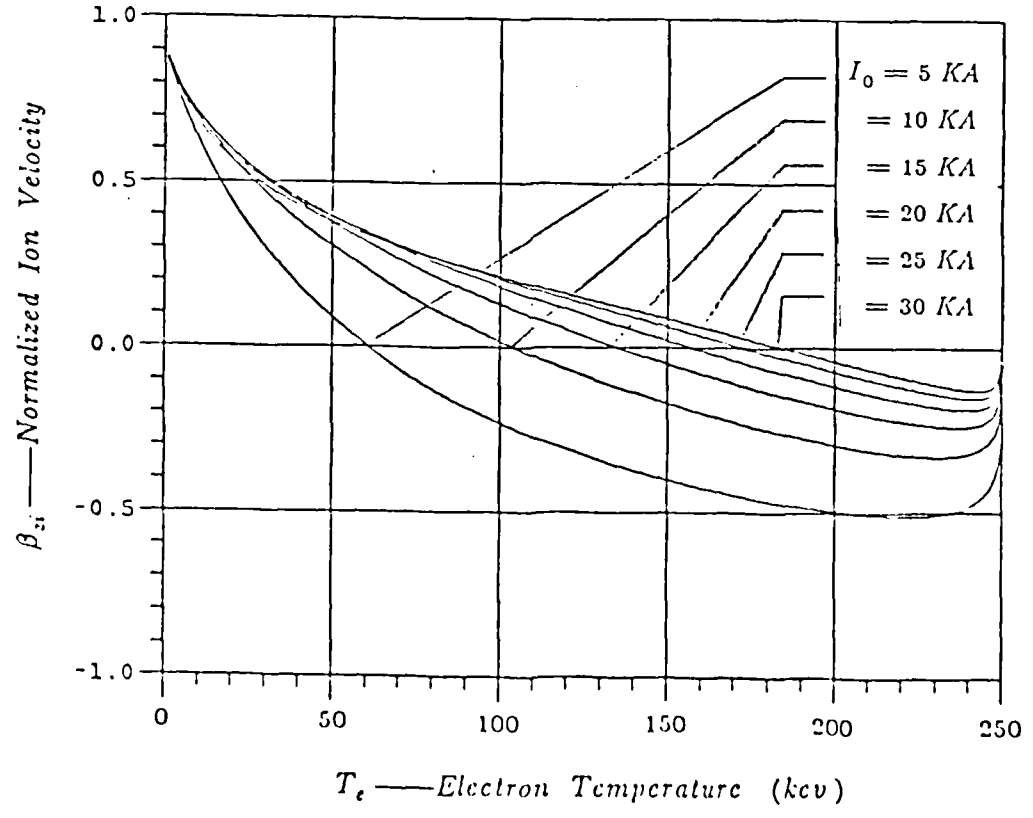

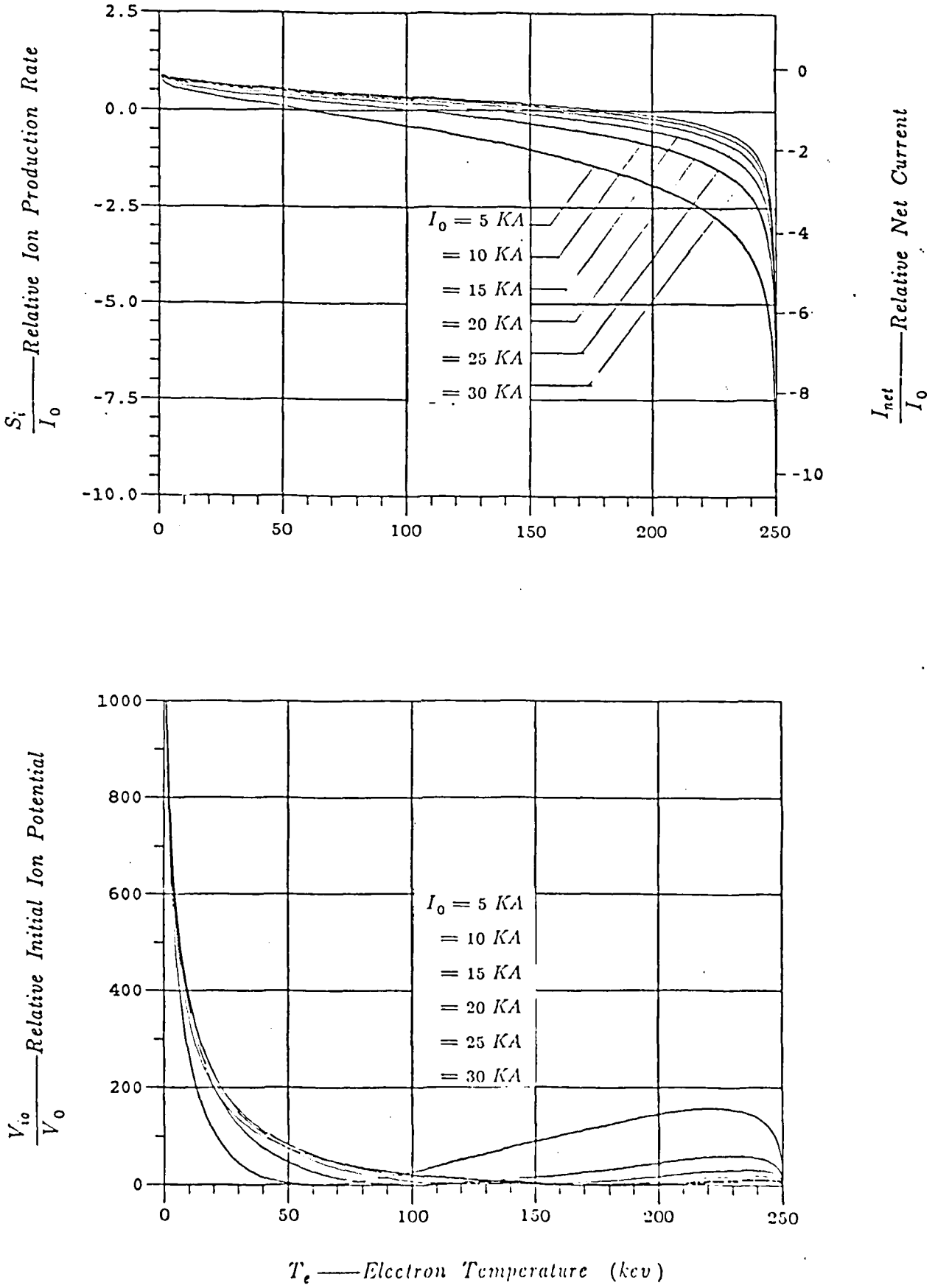
$\frac{S_i}{I_0}$ —Relative Ion Production Rate
$\frac{I_{net}}{I_0}$ —Relative Net Current
$I_0 = 5\ KA$
$= 10\ KA$
$= 15\ KA$
$= 20\ KA$
$= 25\ KA$
$= 30\ KA$
2.5
0.0
-2.5
-5.0
-7.5
-10.0
0
-2
-4
-6
-8
-10
0
50
100
150
200
250
$\frac{V_{io}}{V_0}$ —Relative Initial Ion Potential
1000
800
600
400
200
0
T_e —Electron Temperature (kev)

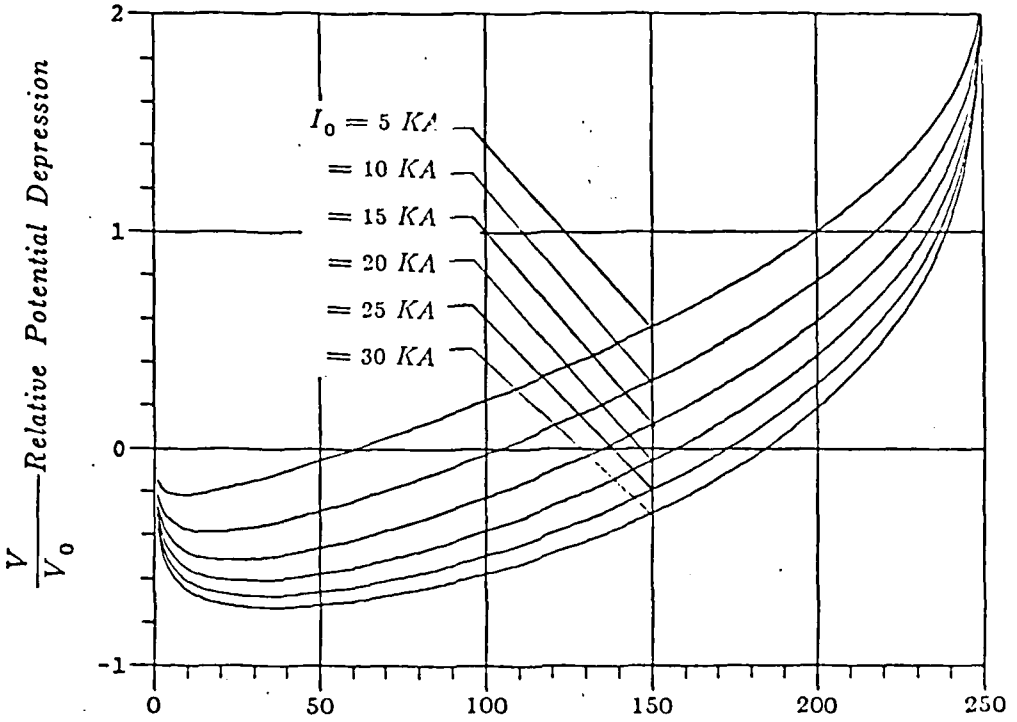
$\frac{V}{V_0}$ —Relative Potential Depression
$I_0 = 5$ KA
= 10 KA
= 15 KA
= 20 KA
= 25 KA
= 30 KA
2
1
0
-1
0
50
100
150
200
250

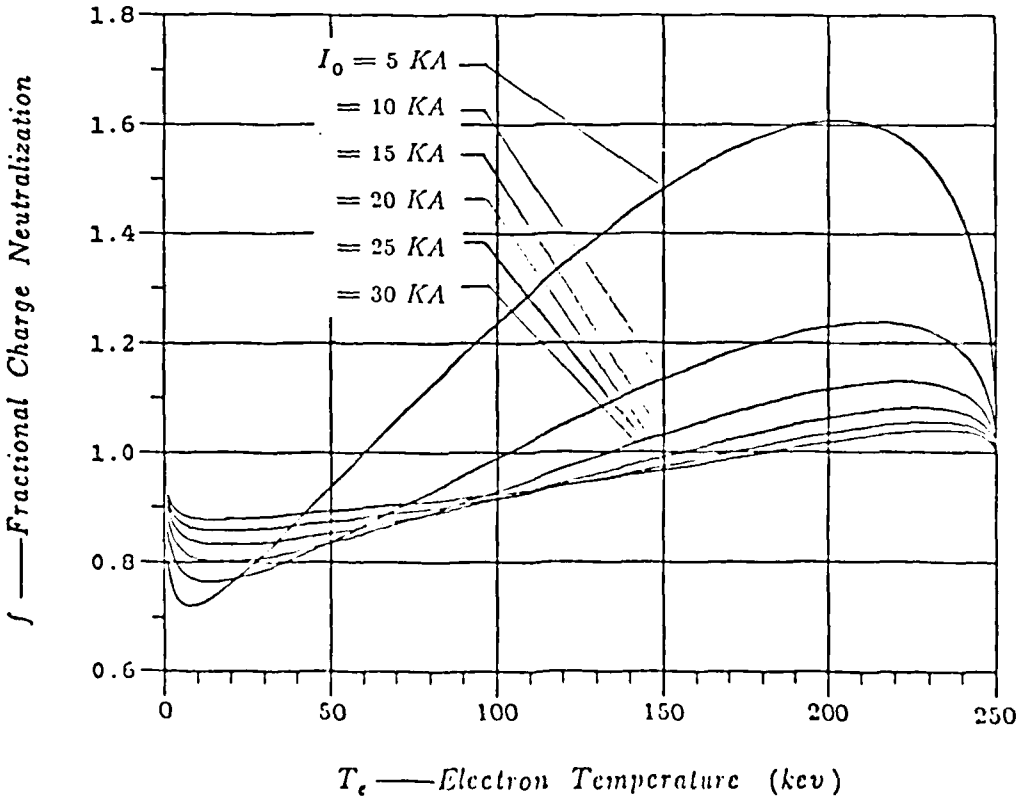
f —Fractional Charge Neutralization
$I_0 = 5$ KA
= 10 KA
= 15 KA
= 20 KA
= 25 KA
= 30 KA
1.8
1.6
1.4
1.2
1.0
0.8
0.6
0
50
100
150
200
250
T_e —Electron Temperature (kev)

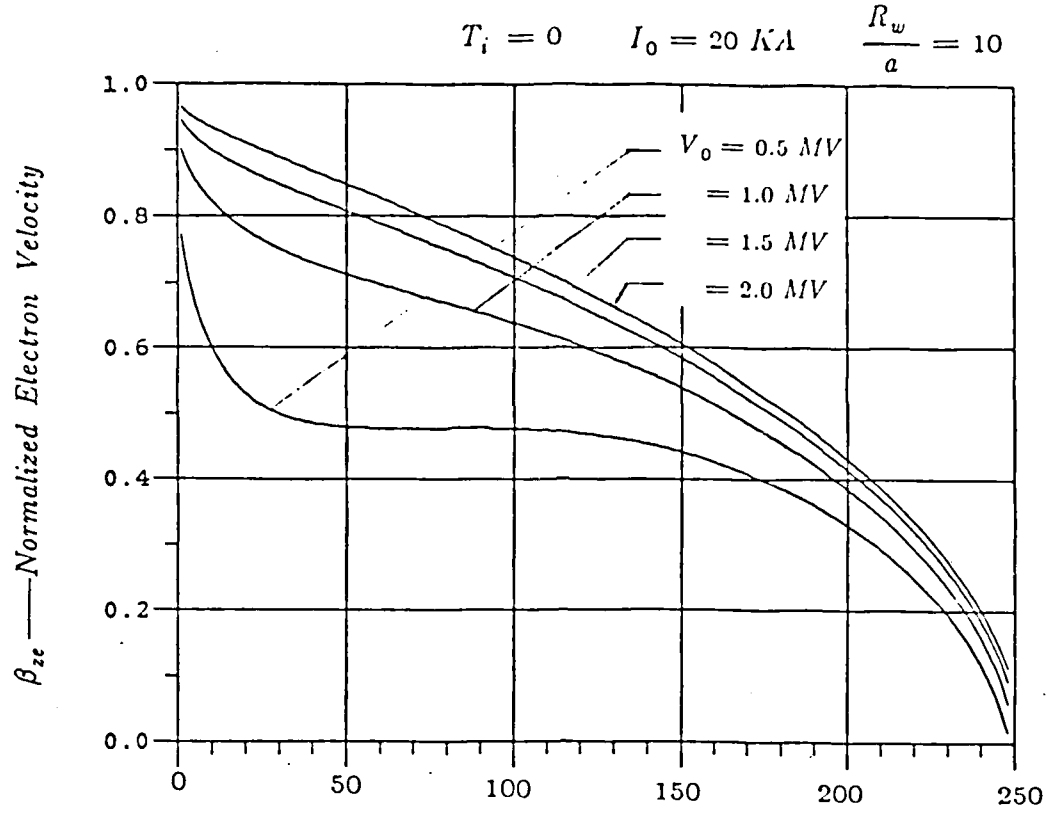
$T_i = 0$
$I_0 = 20\ KA$
$\frac{R_w}{a} = 10$
$V_0 = 0.5\ MV$
$= 1.0\ MV$
$= 1.5\ MV$
$= 2.0\ MV$
1.0
0.8
0.6
0.4
0.2
0.0
0
50
100
150
200
250
β_{ze} ——Normalized Electron Velocity

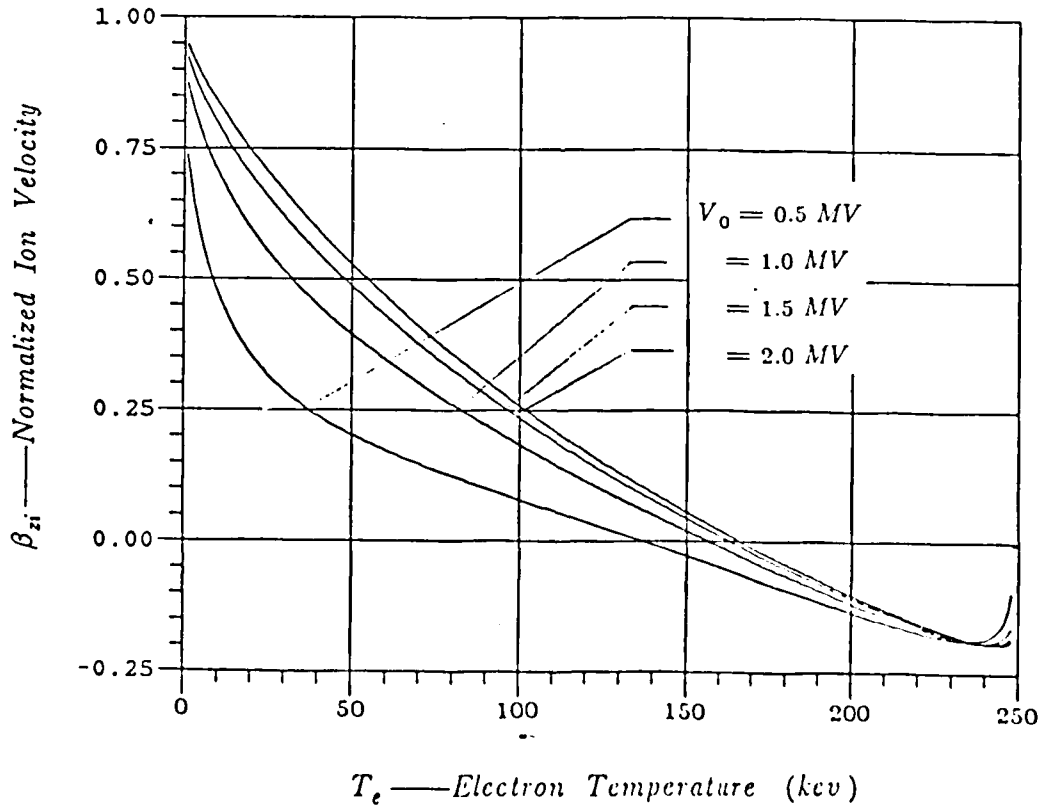
$V_0 = 0.5\ MV$
$= 1.0\ MV$
$= 1.5\ MV$
$= 2.0\ MV$
1.00
0.75
0.50
0.25
0.00
-0.25
0
50
100
150
200
250
β_{zi} ——Normalized Ion Velocity
T_e ——Electron Temperature (kev)

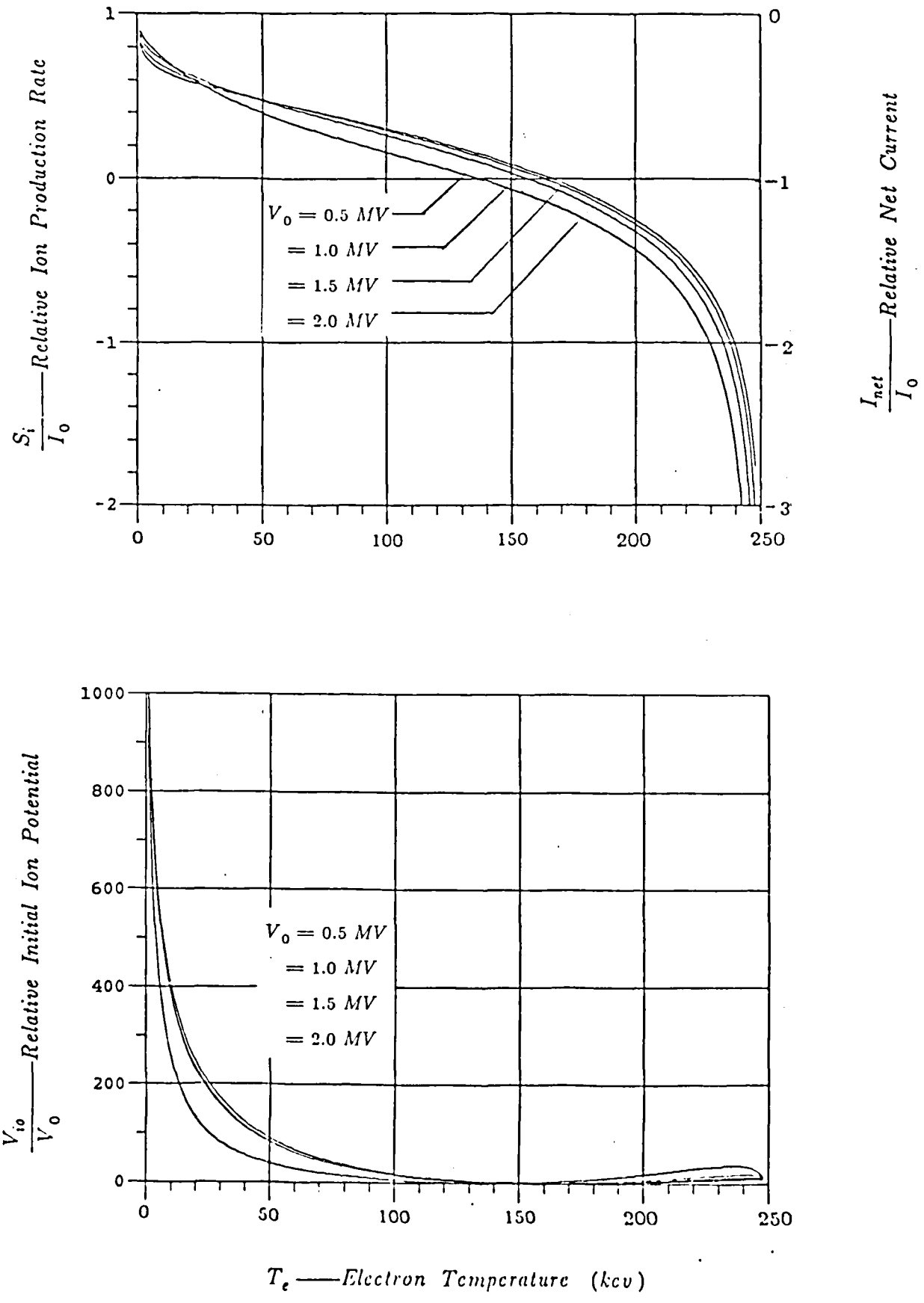
$\frac{S_i}{I_0}$ —Relative Ion Production Rate
$\frac{I_{net}}{I_0}$ —Relative Net Current
$V_0 = 0.5\ MV$
$= 1.0\ MV$
$= 1.5\ MV$
$= 2.0\ MV$
1
0
-1
-2
0
-1
-2
-3
0
50
100
150
200
250
$\frac{V_{i0}}{V_0}$ —Relative Initial Ion Potential
1000
800
600
400
200
0
T_e —Electron Temperature (kev)

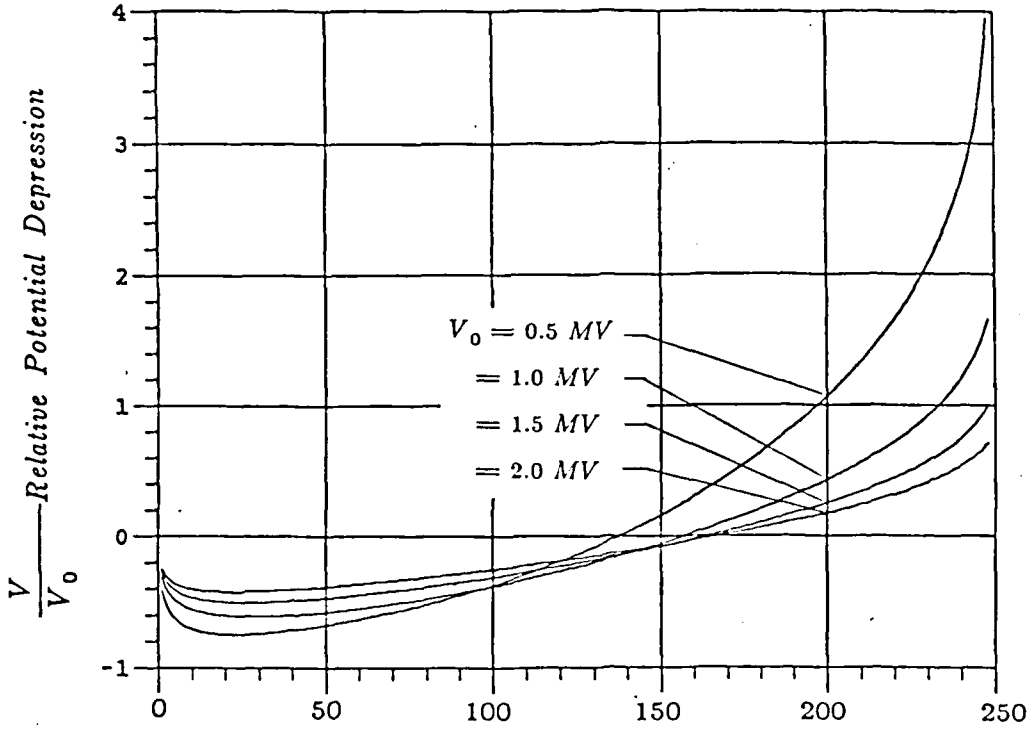
4
3
2
1
0
-1
0
50
100
150
200
250
$V_0 = 0.5\ MV$
$= 1.0\ MV$
$= 1.5\ MV$
$= 2.0\ MV$
$\frac{V}{V_0}$ —Relative Potential Depression

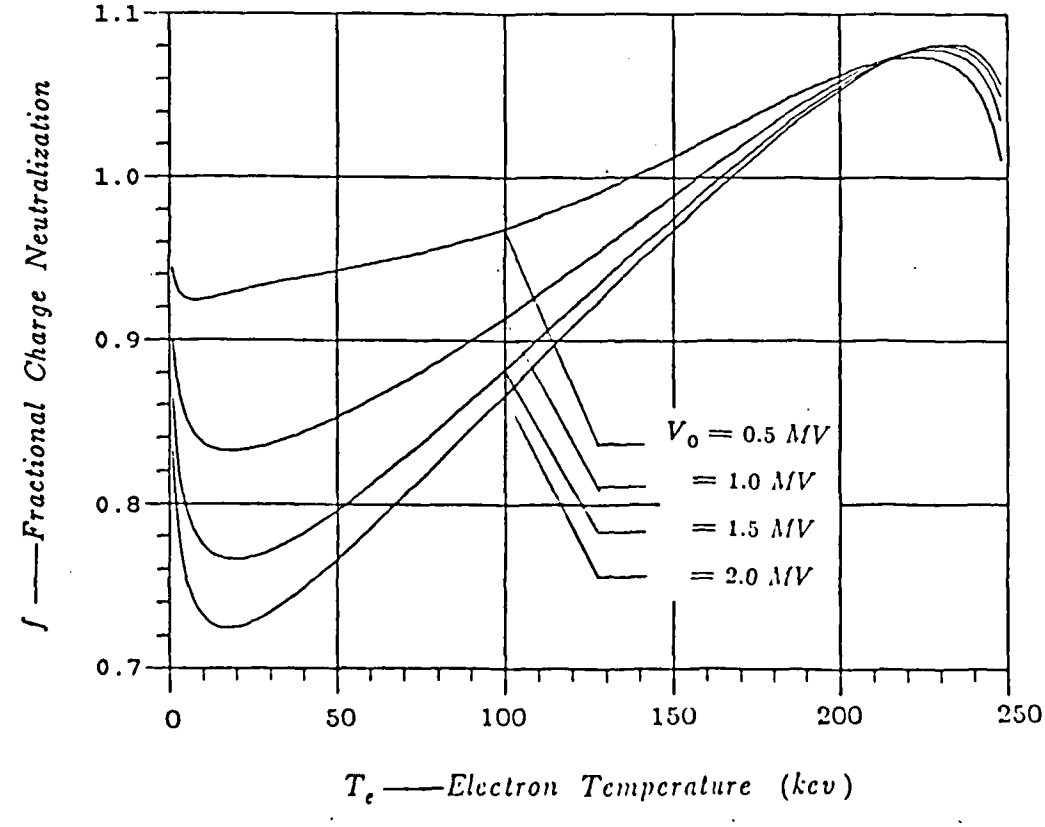
1.1
1.0
0.9
0.8
0.7
0
50
100
150
200
250
$V_0 = 0.5\ MV$
$= 1.0\ MV$
$= 1.5\ MV$
$= 2.0\ MV$
f —Fractional Charge Neutralization
T_e —Electron Temperature (kev)

SPECIAL CASES $T_i = 0$

1. *CHARGE* and *CURRENT NEUTRALIZED LIMIT* —— $T_e = 0$

For $n_0 \neq 0$, *need* $\beta_{ze} = \beta_{zi}$.

$$zn_i = \left(\frac{1 - \beta_{zi}\beta_{ze}}{1 - \beta_{zi}^2}\right) n_e = n_e$$

$$V(0) = 0, \qquad \gamma_e = \gamma_i$$

$$\frac{V_{i0}}{V_0} = \frac{m_i}{m_e} = 1836$$

$$S_i = I_0$$

2. *CHARGE NEUTRALIZED LIMIT* —— $\beta_{zi} = 0$

$$n_0 = \frac{8\pi K T_e}{e^2 a^2} \frac{1}{\beta_{ze}^2}$$

$$zn_i = \frac{1 - \beta_{ze}\beta_{zi}}{1 - \beta_{zi}^2} n_e = n_e$$

$$V(0) = 0$$

$$S_i = 0$$

$$I_0 = \frac{8\pi\epsilon_0 c K T_e^*}{\beta_{ze}^* e}$$

$$\gamma_e = \frac{1}{\sqrt{1 - \beta_{te}^2 - \beta_{ze}^{*2}}}$$

$$\frac{KT_e^*}{e} \approx \frac{I_0\beta_0}{8\pi\epsilon_0 c} - \frac{eI_0^2}{128\pi^2\epsilon_0^2 c^4 m_e} + \frac{c^2 I_0^3}{4096\pi^3\epsilon_0^3 c^7 m_e^2 \beta_0}$$

$\frac{R_w}{a} = 10 \qquad T_i = 0$

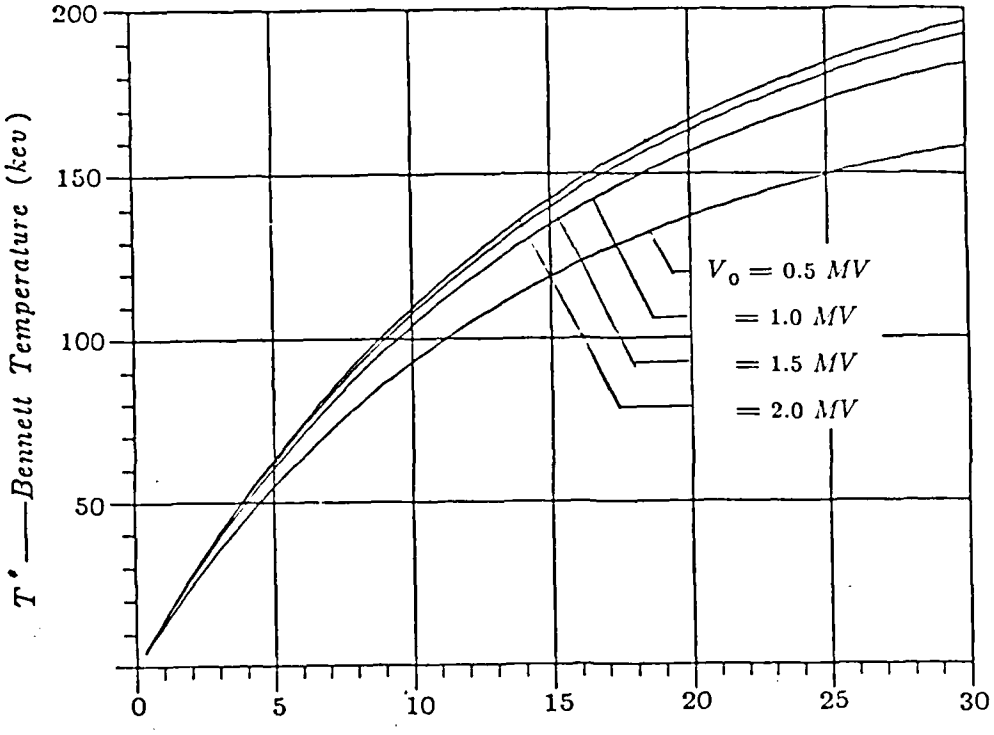

$T_i = 40$ kev

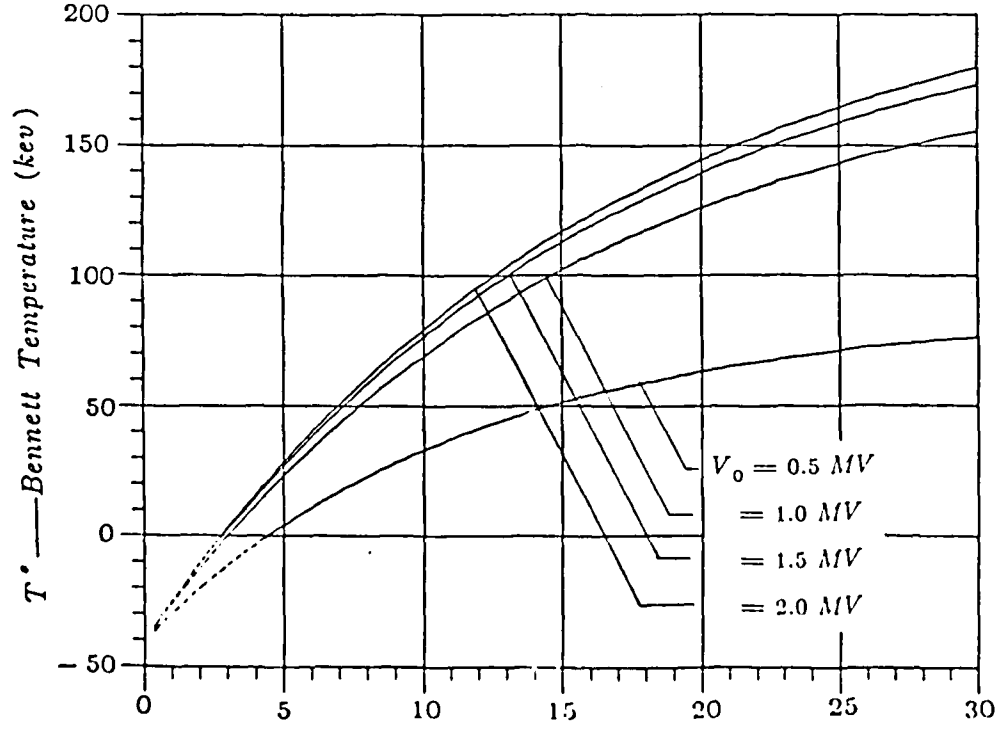

Equilibrium Results ($T_i \neq 0$)

$I_0 = 20\ KA \quad V_0 = 1.0\ MV \quad \frac{R_w}{a} = 10$

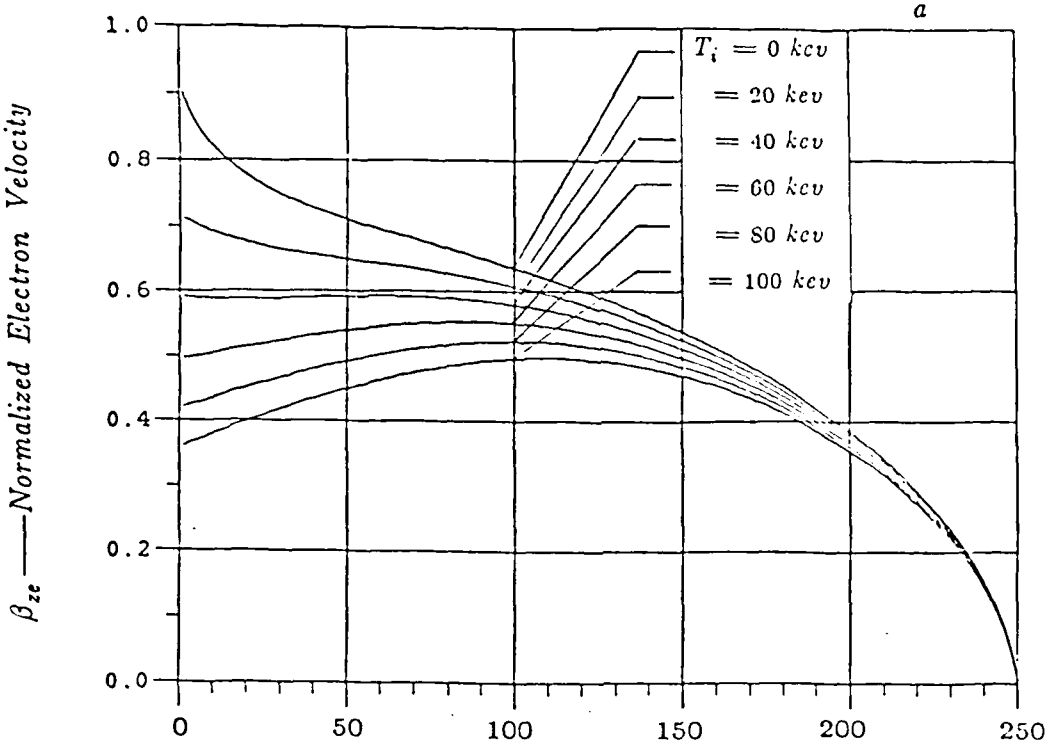

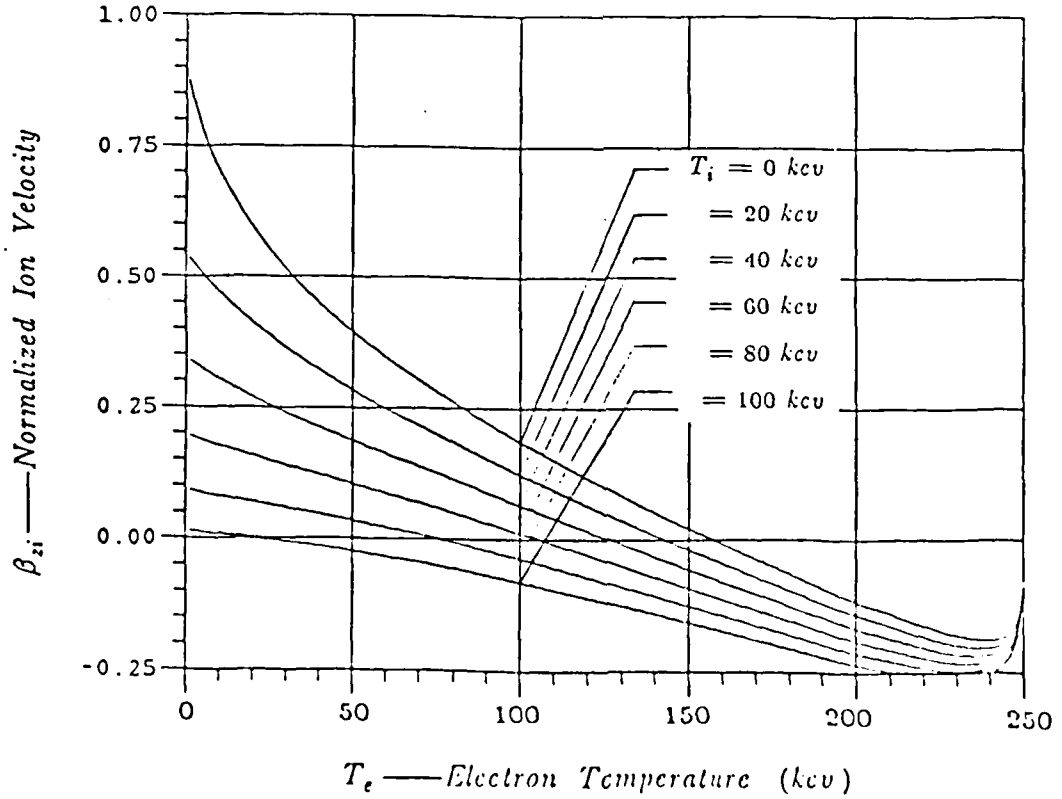

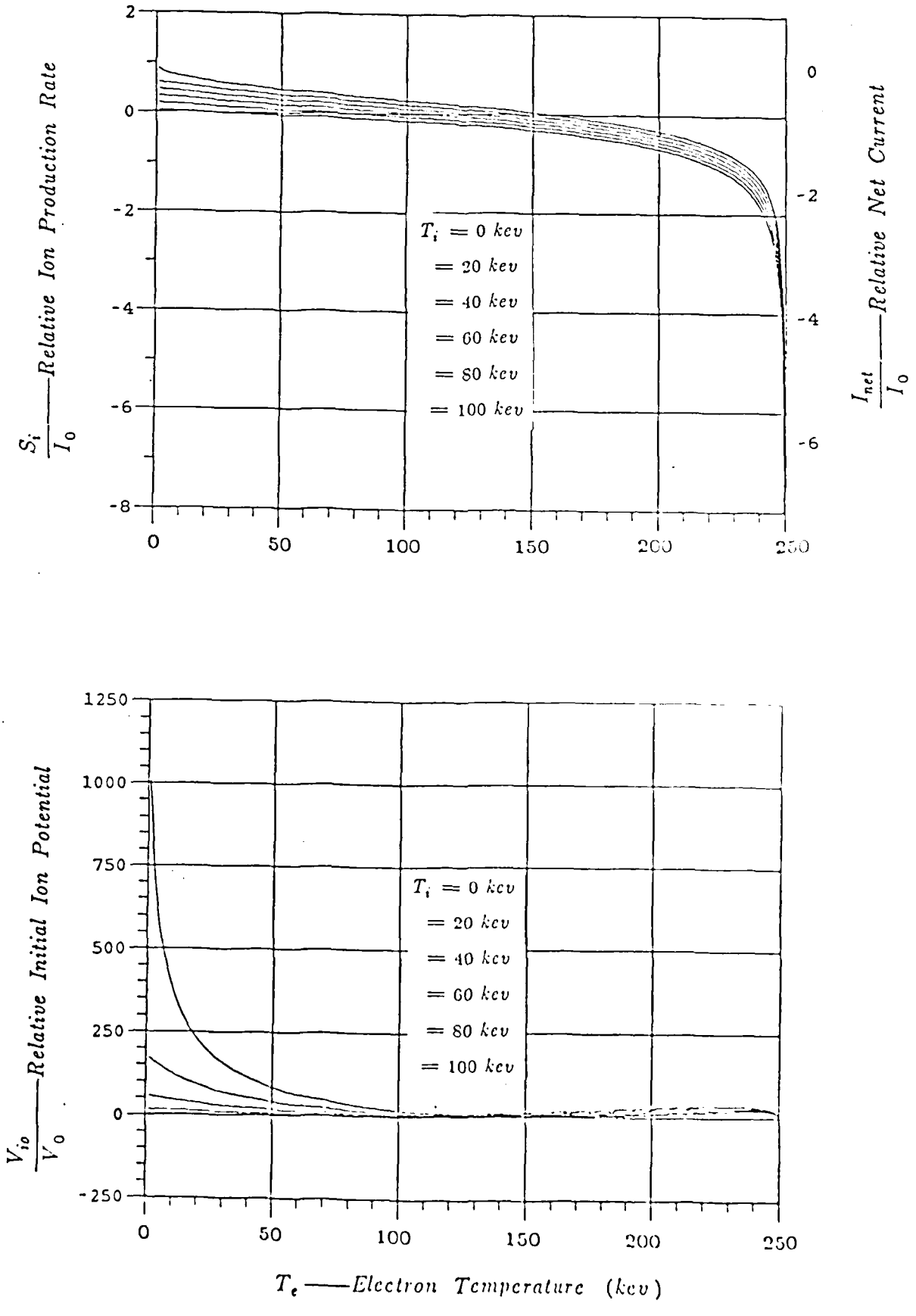
$\frac{S_i}{I_0}$ —Relative Ion Production Rate
$\frac{I_{net}}{I_0}$ —Relative Net Current
T_i = 0 kev
= 20 kev
= 40 kev
= 60 kev
= 80 kev
= 100 kev
2
0
-2
-4
-6
-8
0
50
100
150
200
250
$\frac{V_{io}}{V_0}$ —Relative Initial Ion Potential
1250
1000
750
500
250
0
-250
T_e —Electron Temperature (kev)

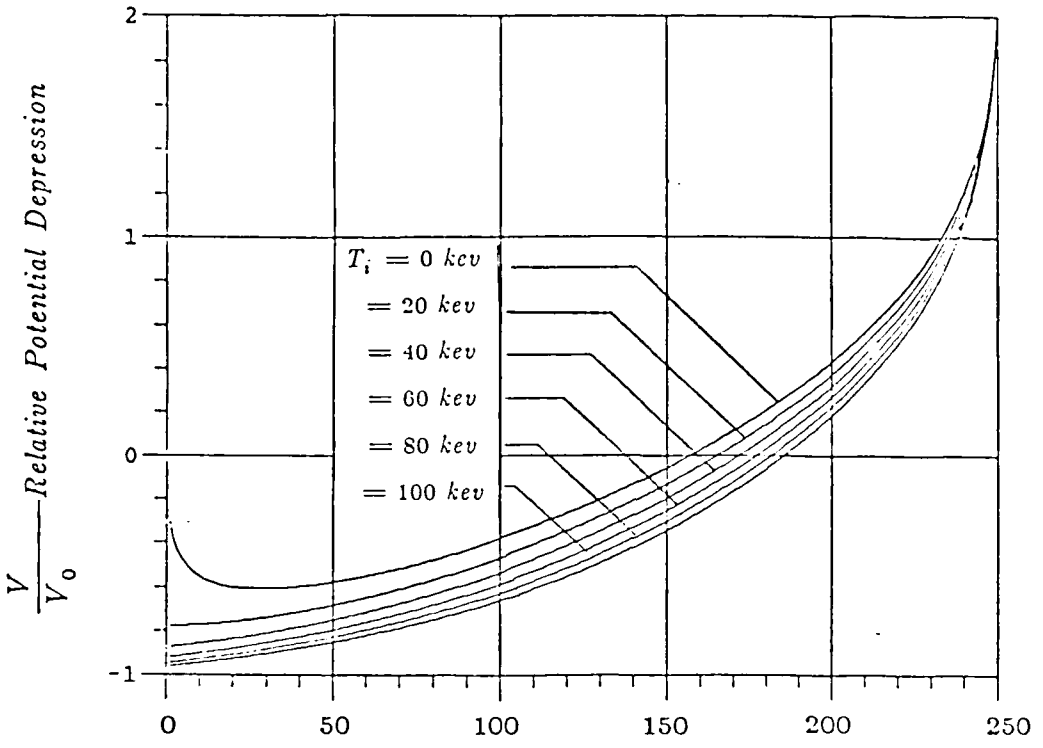
2
1
0
-1
0
50
100
150
200
250
T_i = 0 kev
= 20 kev
= 40 kev
= 60 kev
= 80 kev
= 100 kev
$\frac{V}{V_0}$ —Relative Potential Depression

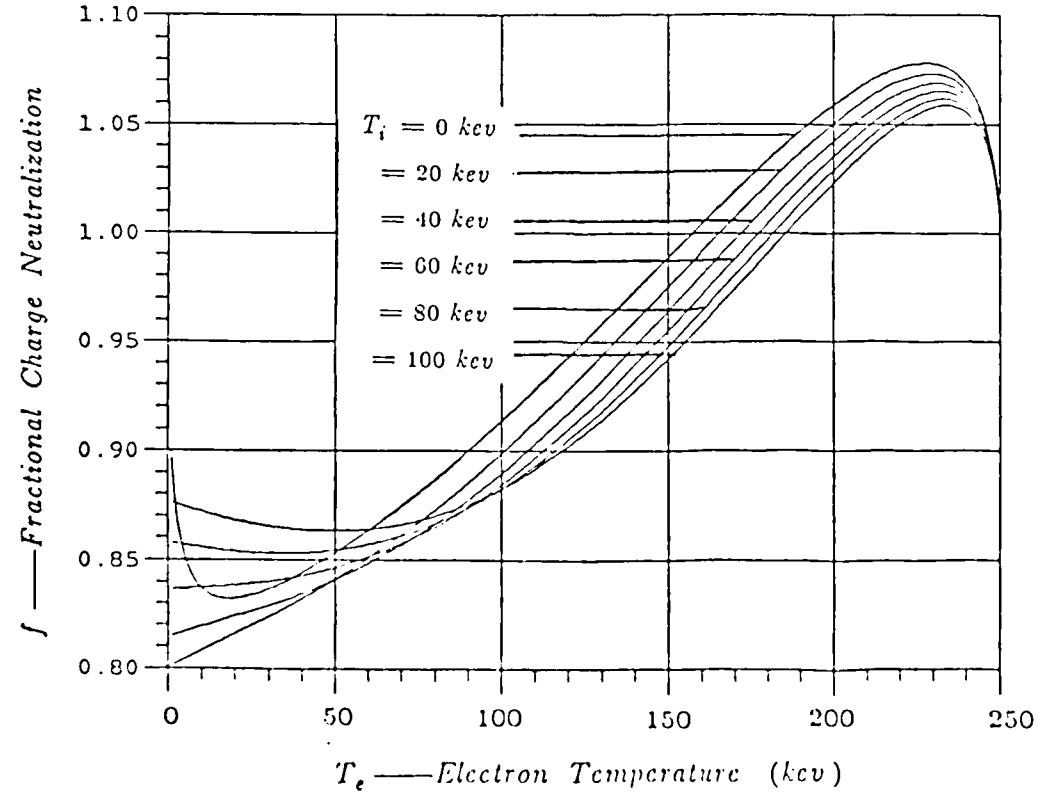
1.10
1.05
1.00
0.95
0.90
0.85
0.80
0
50
100
150
200
250
T_i = 0 kev
= 20 kev
= 40 kev
= 60 kev
= 80 kev
= 100 kev
f —Fractional Charge Neutralization
T_e —Electron Temperature (kev)

Realistic Pulse Shape Results

From simulation results of gas cloud ionization [Dantsker etal, Bull. APS 29, 1353(1984)]:

$$\frac{S_i}{I_0(t)} \leq 0.1 \quad \text{and} \quad \frac{V_{i0}}{V_0} \leq 1$$

Using these results and $\beta_{zi} \geq 0$, *can determine the realistic pulse shape.*

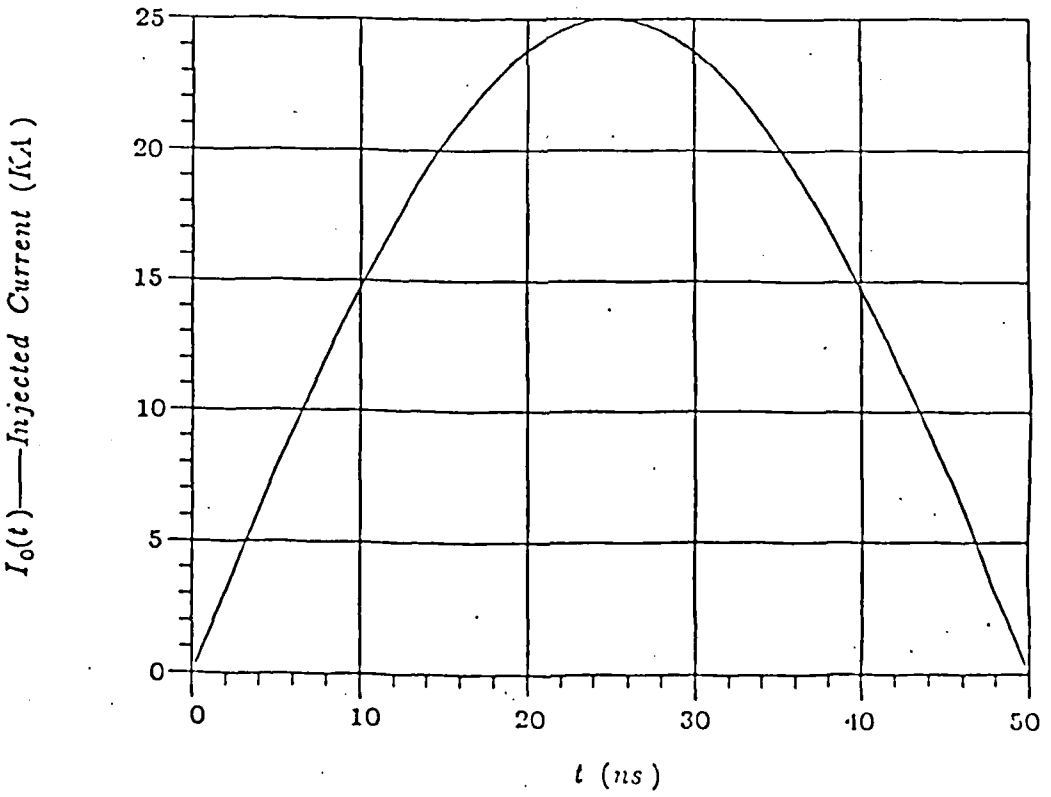

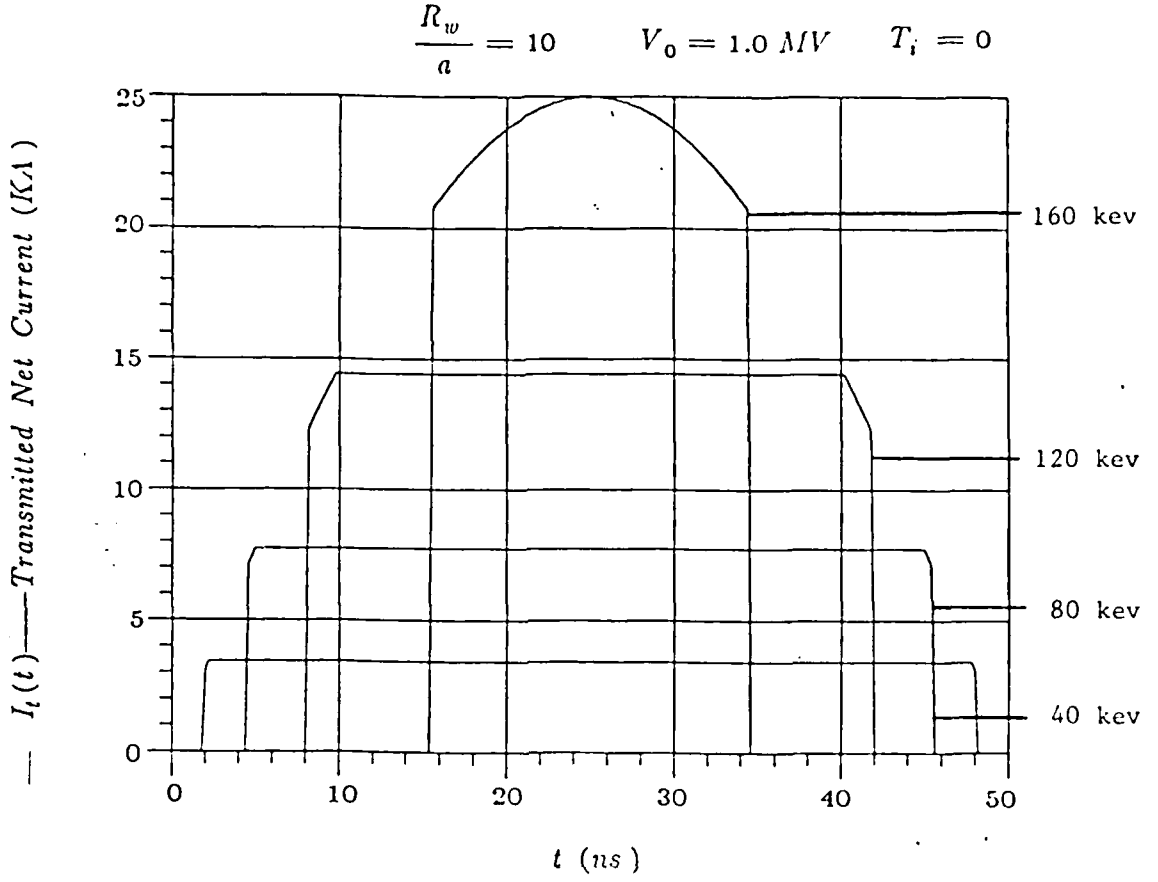
$\frac{R_w}{a} = 10$
$V_0 = 1.0\ MV$
$T_i = 0$
$I_t(t)$——Transmitted Net Current (KA)
25
20
15
10
5
0
0
10
20
30
40
50
160 kev
120 kev
80 kev
40 kev
t (ns)

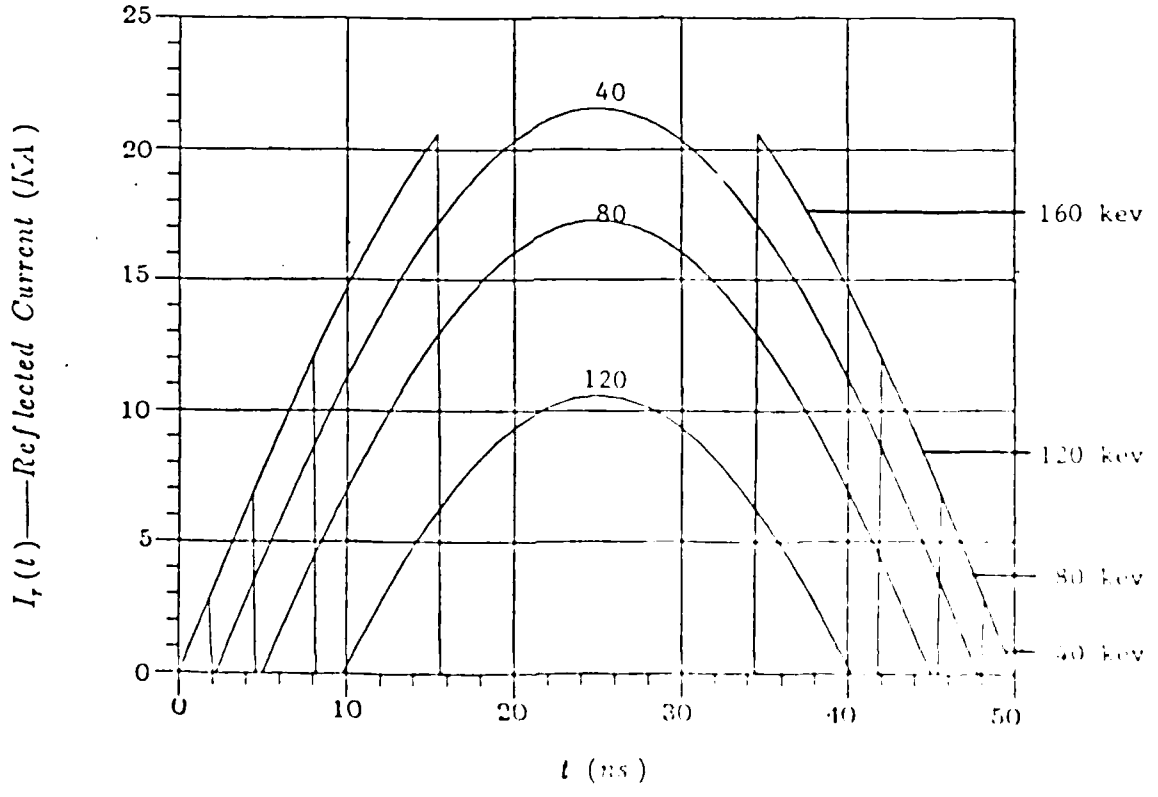
$I_r(t)$——Reflected Current (KA)
25
20
15
10
5
0
0
10
20
30
40
50
40
80
120
160 kev
120 kev
80 kev
40 kev
t (ns)

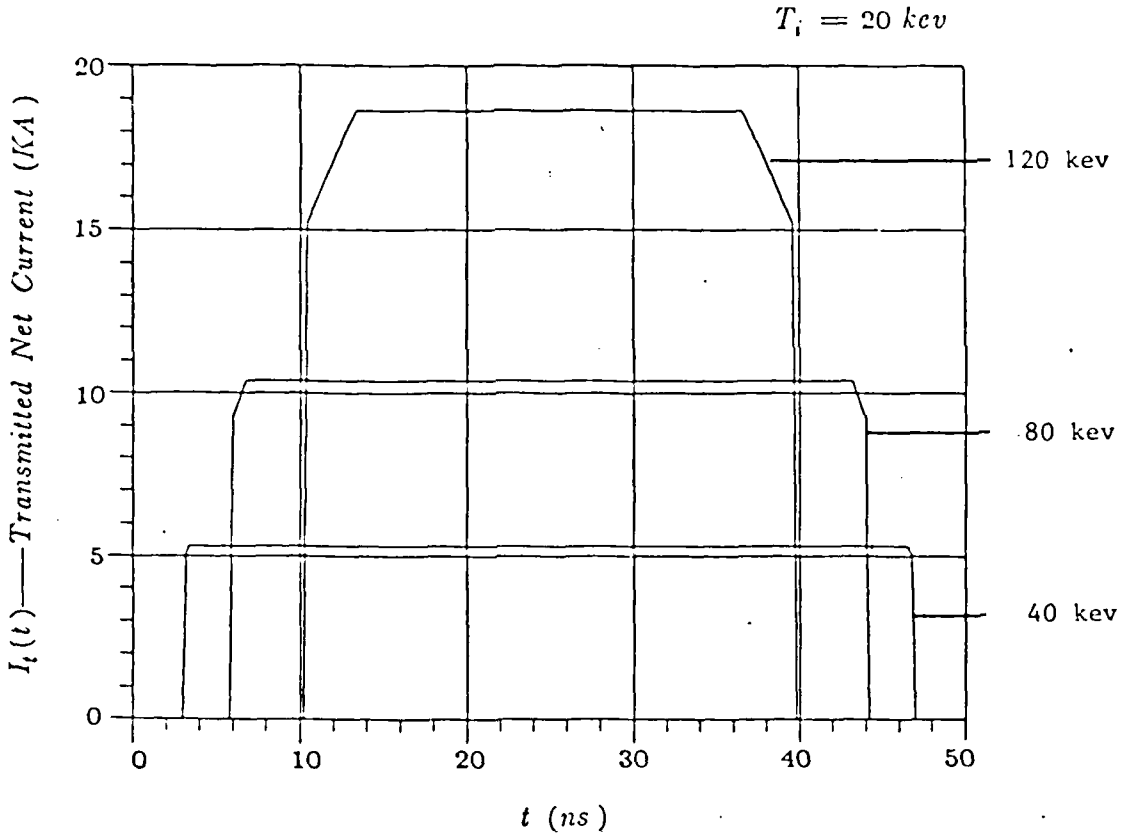
$T_i = 20\ kev$
$I_t(t)$——Transmitted Net Current (KA)
20
15
10
5
0
0
10
20
30
40
50
t (ns)
120 kev
80 kev
40 kev

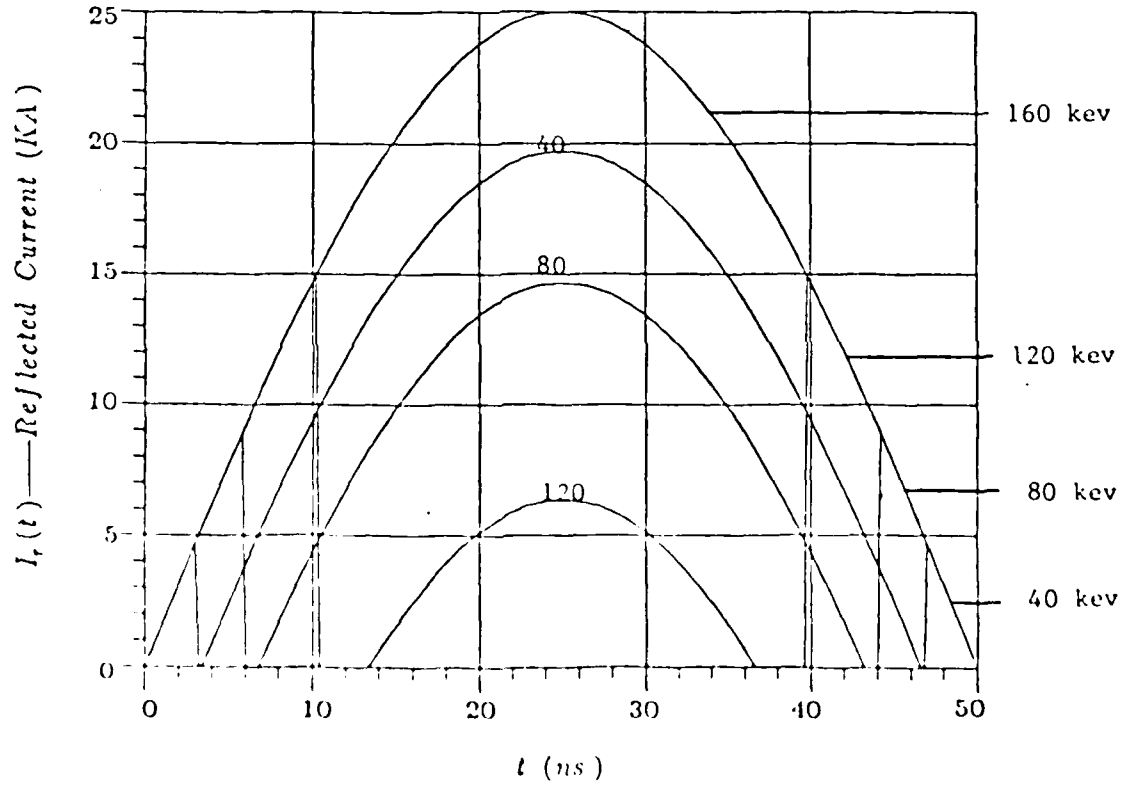
$I_r(t)$——Reflected Current (KA)
25
20
15
10
5
0
0
10
20
30
40
50
t (ns)
40
80
120
160 kev
120 kev
80 kev
40 kev

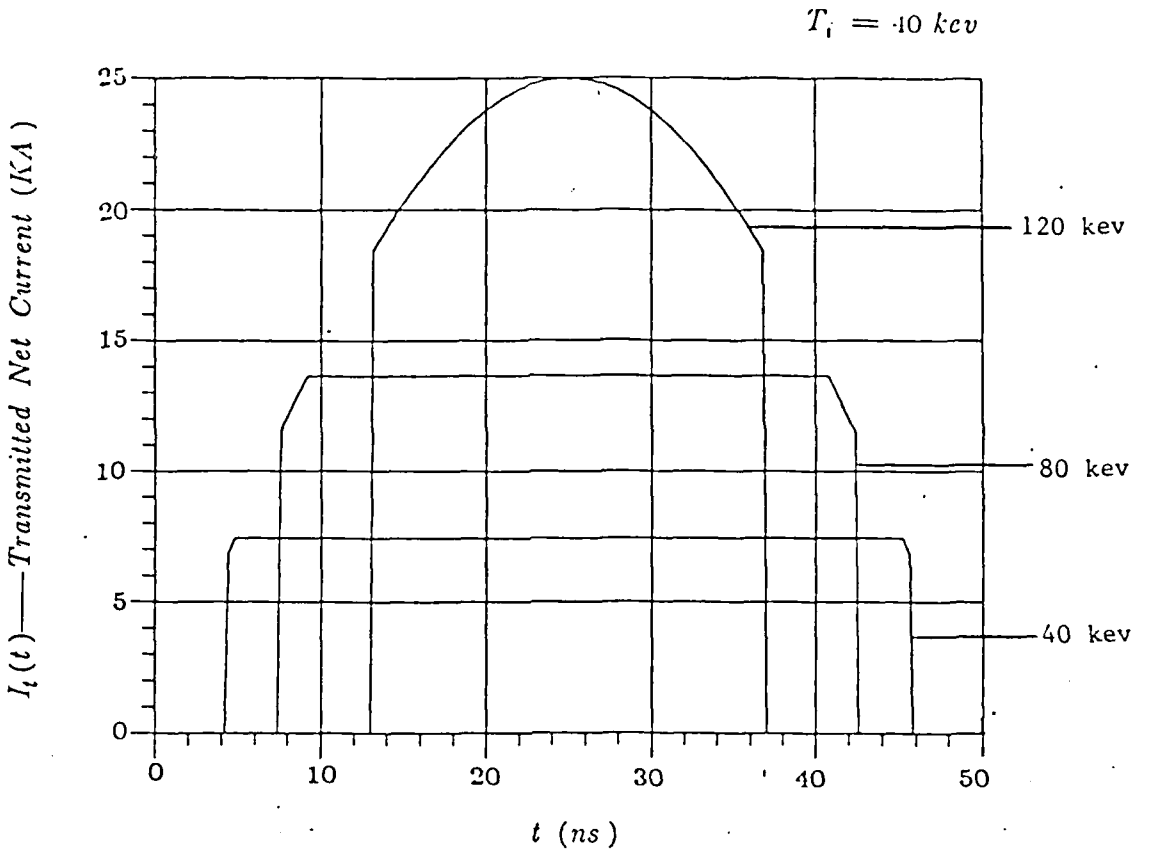
$T_i = 10$ kev
$I_t(t)$——Transmitted Net Current (KA)
25
20
15
10
5
0
0
10
20
30
40
50
t (ns)
120 kev
80 kev
40 kev

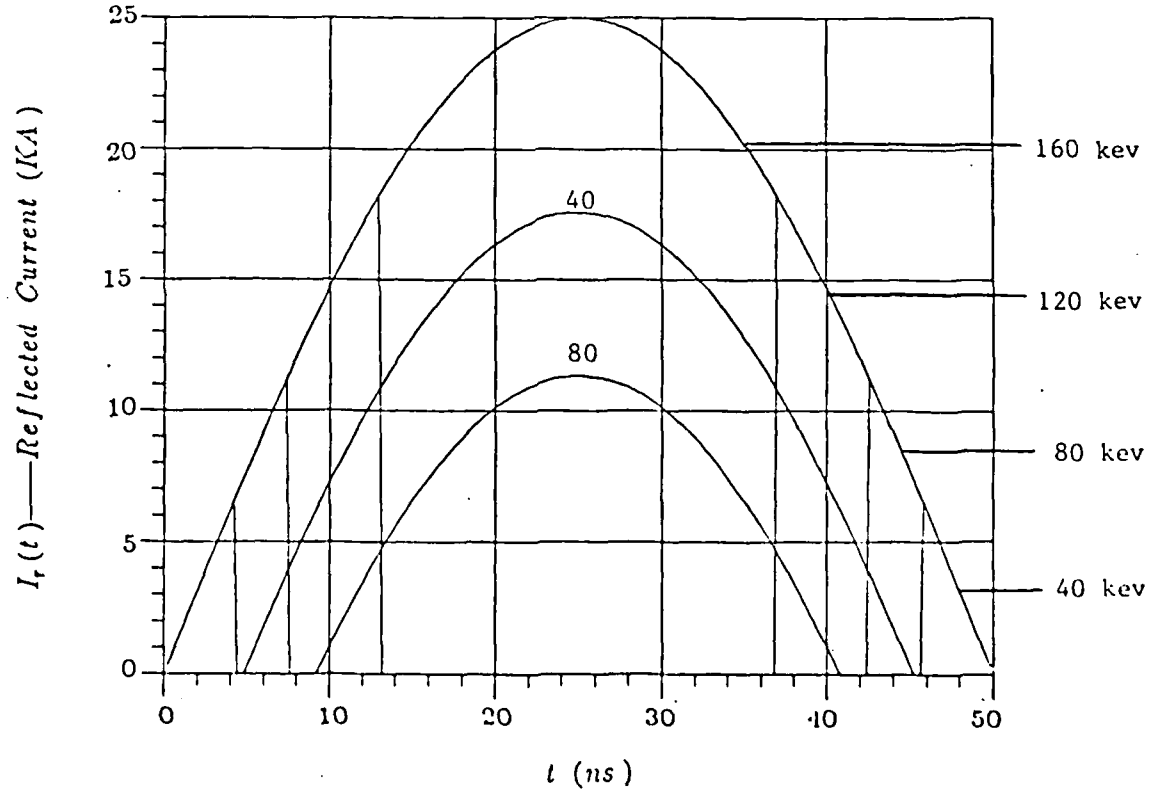
$I_r(t)$——Reflected Current (KA)
25
20
15
10
5
0
0
10
20
30
40
50
t (ns)
160 kev
120 kev
80 kev
40 kev
40
80

Conclusions

1. A self-consistant downstream equilibrium exists between electrons and ions with no axial magnetic field. The electrons are confined by the self magnetic field and the ions by the self electric field.

2. $\underline{T_i = 0}$ A temperature $T_e = T_e^* (\beta_{zi} = 0)$ exists where $f = 1$ and $I_{net} = I_0$ (charge neutral-Bennett system). A parameter regime in T_e exists where the system is nearly charge neutralized and the net current is nearly the injected electron beam current for a given I_0, V_0. This regime is $T_e \leq T_e^*$. By increasing the diode voltage and the injected current T_e^* will move to higher values.

3. $\underline{T_i \neq 0}$ The effect of ion temperature T_i makes $T_e^* (\beta_{zi} = 0)$ move to lower values. Furthermore, there is no charge neutral and/or current neutral points in regime $T_e \leq T_e^*$.

4. The realistic transmitted pulse shapes change with electron temperature and ion temperature. Pulses become narrower but allow more net current when temperature increases up to $T_e^*(I_m)$ ---- no current can be transmitted and injected current is totally reflected.

END

5-87

DTIC